387498

THE INELASTIC BUCKLING STRENGTH OF FABRICATED HY-80 STEEL HEMISPHERICAL SHELLS   Report 2304

NAVAL SHIP RESEARCH AND DEVELOPMENT CENTER

THE INELASTIC BUCKLING STRENGTH OF FABRICATED HY-80 STEEL HEMISPHERICAL SHELLS

by

M.G. Costello and K. Nishida

Distribution of this document is unlimited

STRUCTURAL MECHANICS LABORATORY
RESEARCH AND DEVELOPMENT REPORT

April 1967

Report 2304

THE INELASTIC BUCKLING STRENGTH OF FABRICATED HY-80 STEEL HEMISPHERICAL SHELLS

by

M.G. Costello and K. Nishida

Distribution of this document is unlimited

April 1967

Report 2304
S-F013 01 03, Task 0214
S-F013 03 02, Task 1900

TABLE OF CONTENTS

LIST OF FIGURES

LIST OF TABLES

ABSTRACT

Eight, 66-in.-diameter, fabricated HY-80 steel hemispherical shells designed to fail by inelastic buckling were tested to observe the effects of initial imperfections and residual stresses on elastic behavior and collapse strength. The results demonstrate that the effect of secondary moments and residual stresses on collapse strength diminish as the ratio of elastic to inelastic buckling pressure increases. It was possible to predict the collapse pressures of these models within ± 10 percent by utilizing imperfection analysis and extrapolating previous test results of less stable shells. Fairly good agreement was also obtained by using the same imperfection analysis to predict the membrane stresses in the center of the flat spots. Addition of the results of these tests to those obtained on shells in the less stable regions provides a basis for a reasonable collapse equation for practical spherical shells over the range of shell stability of interest to deep submergence.

ADMINISTRATIVE INFORMATION

The work described in this report was conducted under the sponsorship of the Special Projects Office, Subproject S-F013 01 03, Task 0214, and the Naval Ships Systems Command, Subproject S-F013 03 02, Task 1960.

INTRODUCTION

The lack of adequate criteria for designing fabricated spherical shells under hydrostatic loading has been a problem to designers for many years. It is well known that under such loading the elastic buckling strength is considerably less than predicted by classical linear theory. The lower strength is generally attributed to the effects of initial imperfections, residual stresses, and adverse boundary conditions which the theory neglects. Thus, in the absence of adequate criteria, designers have had to resort to high factors of safety and to accept the associated weight penalties.

Interest in deeper diving submarines and small research vehicles has emphasized the need for more adequate criteria. In the past few years, the David Taylor Model Basin has conducted extensive studies of machined shells to develop the necessary background.[1-4] These led to development of an analysis for near-perfect and initially imperfect, stress-free spherical shells.[5] The investigations were subsequently extended to realistic, large-scale fabricated shells in a parametric study of the buckling strength of HY-80 steel hemispheres.[6] On the basis of these tests, a collapse equation for fabricated shells was proposed, by which collapse strength would be calculated on the basis of measured local imperfection geometry. In the course of this study, it became evident that further tests of more stable shells were required. Thus, eight additional models were designed to investigate the behavior of spherical shells possessing a ratio of elastic-to-inelastic collapse strength of about 2.5 to 4.0. This report discusses the fabrication, test procedures, and results for these eight models.

DESCRIPTION OF MODELS

The eight, 66-in.-diameter, hemispherical shell models were fabricated by the Lukens Steel Company from HY-80 steel (nominal yield strength of 80,000 psi). Each model consisted of seven pressed and welded segments; six, 60-deg, orange-peel segments and a 60-deg polar cap. Four of the models (Models 75, 76, 79, and 80) had a nominal thickness to radius h/R ratio of 0.024 and the other four (Models 77, 78, 81, and 82) had an h/R ratio of 0.030. Models 76, 80, 78, and 82 were tested in the as-fabricated condition; Models 75, 79, 77, and 81 were tested after stress relieving. In stress relieving the model, the furnace was preheated to a temperature of 1025 F. The model was then inserted in the furnace and stress relieved for 1 hour, after which the model was removed from the furnace and air cooled.

An internally ring-stiffened cylinder was welded to each model prior to testing. Because of the tolerances involved in fabricating spherical shells of this size and the need to employ nominal dimensions in design, it was not practical to utilize cylinders that would ensure membrane

---

[1] References are listed on page 40.

boundaries at the juncture of hemisphere and cylinder. Thus, each plating of the cylinder shell was arbitrarily increased in thickness by approximately 10 percent over that which would provide membrane conditions. Figure 1 shows a model and cylinder assembly and presents nominal model dimensions.

In all calculations, Young's modulus E and Poisson's ratio v were assumed to be 30 by 10^6 psi and 0.3, respectively. Yield strengths as determined from uniaxial compression tests of the original plate material are presented in Table 1. For the stress-relieved models, the coupons cut from the original plate were stress-relieved along with the models. In all tests, the specimens were 1/2 in. in diameter by 2 in. in length. A typical stress-strain curve of the original plate material of Model 82 (not stress relieved) is presented in Figure 2. In addition to these tests, samplings of yield strength were taken from Model 82 after the hydrostatic test to observe the effect of forming on strength. Locations of specimens and results are presented in Figure 3. Typical stress-strain curves from three different areas of the segment are presented in Figure 2.

PROCEDURE

DETERMINATION OF INITIAL IMPERFECTIONS

The analysis[5] for initially imperfect, stress-free spherical shells requires the accurate determination of initial imperfections over the entire surface of the shell. It was therefore necessary to take approximately 1000 radius measurements on each model from a fixed point within the shell to the inside surface. The results of these measurements are presented in the form of contour maps (Figure 4) that represent the inside view of a hemisphere unfolded into a flat surface whose radial scale remains constant. This scale can be determined by dividing one-half the circumference of the sphere by the diameter of the contour map. As in the case with the problem of mapping, the scale in all other directions varies, depending on the distance from the center of the plot and the orientation with the radial direction. To overcome this problem, arc-length scales were utilized together with the contour maps for out-of-roundness analysis. A typical arc-length scale is presented in Figure 5.

(Text continued on page 17.)

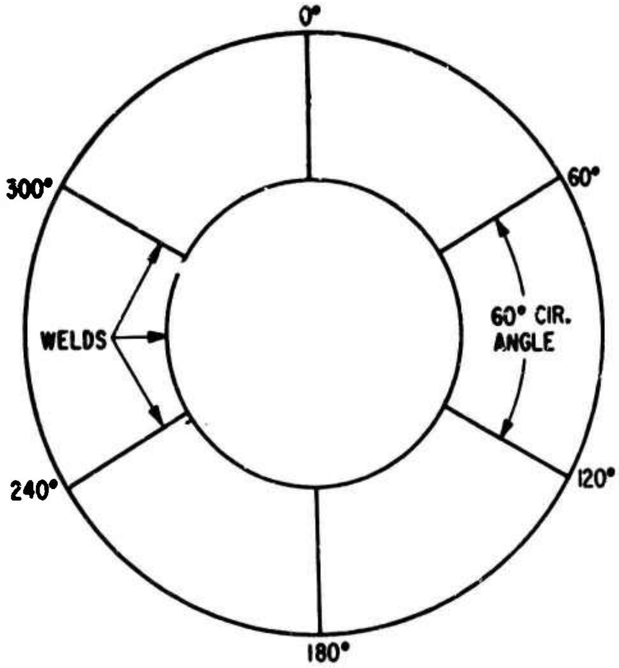

Dimension	Models 75,* 76 79,* 80	Models 77,* 78 81,* 82
a	3 1/4	3 3/8
b	1 1/4	1 3/8
c	1 1/8	1 5/16
d	16 3/4	17 5/8
e	1 1/8	1 5/16
f	2 1/2	2 3/4
g	64 5/8	64 9/16
h_s	13/16	1
j	3 3/4	4 1/8
k	58 1/2	57 3/4

*Stress Relieved

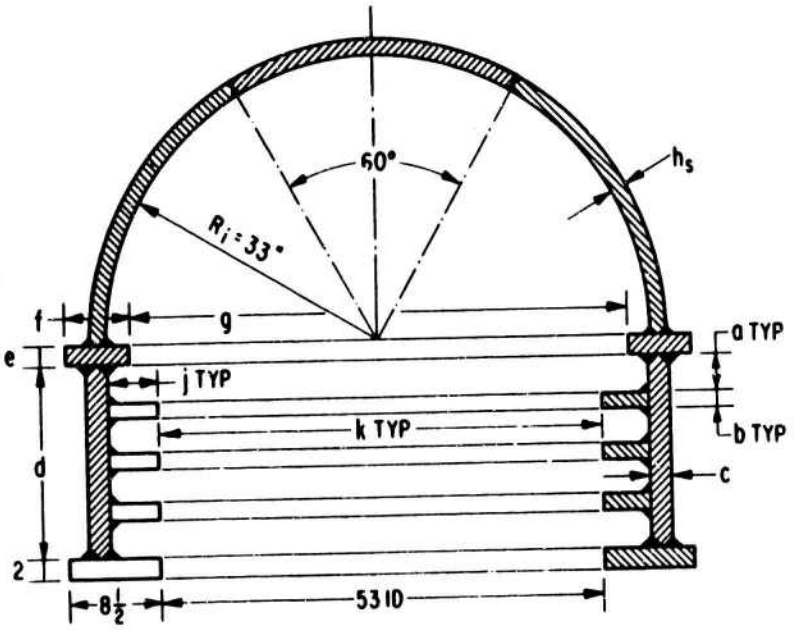

Figure 1 - Model and Cylinder Assembly

TABLE 1

Compressive Yield Strengths

Model	Yield Strength[*] Pounds per Square Inch
75**	87,500
79**	87,500
76	87,600
80	87,600
77**	87,700
81*	87,700
78	92,700
82	92,700

[*] Yield strengths for stress-relieved models determined from specimens which were stress relieved with model.

[**] Indicates stress-relieved models.

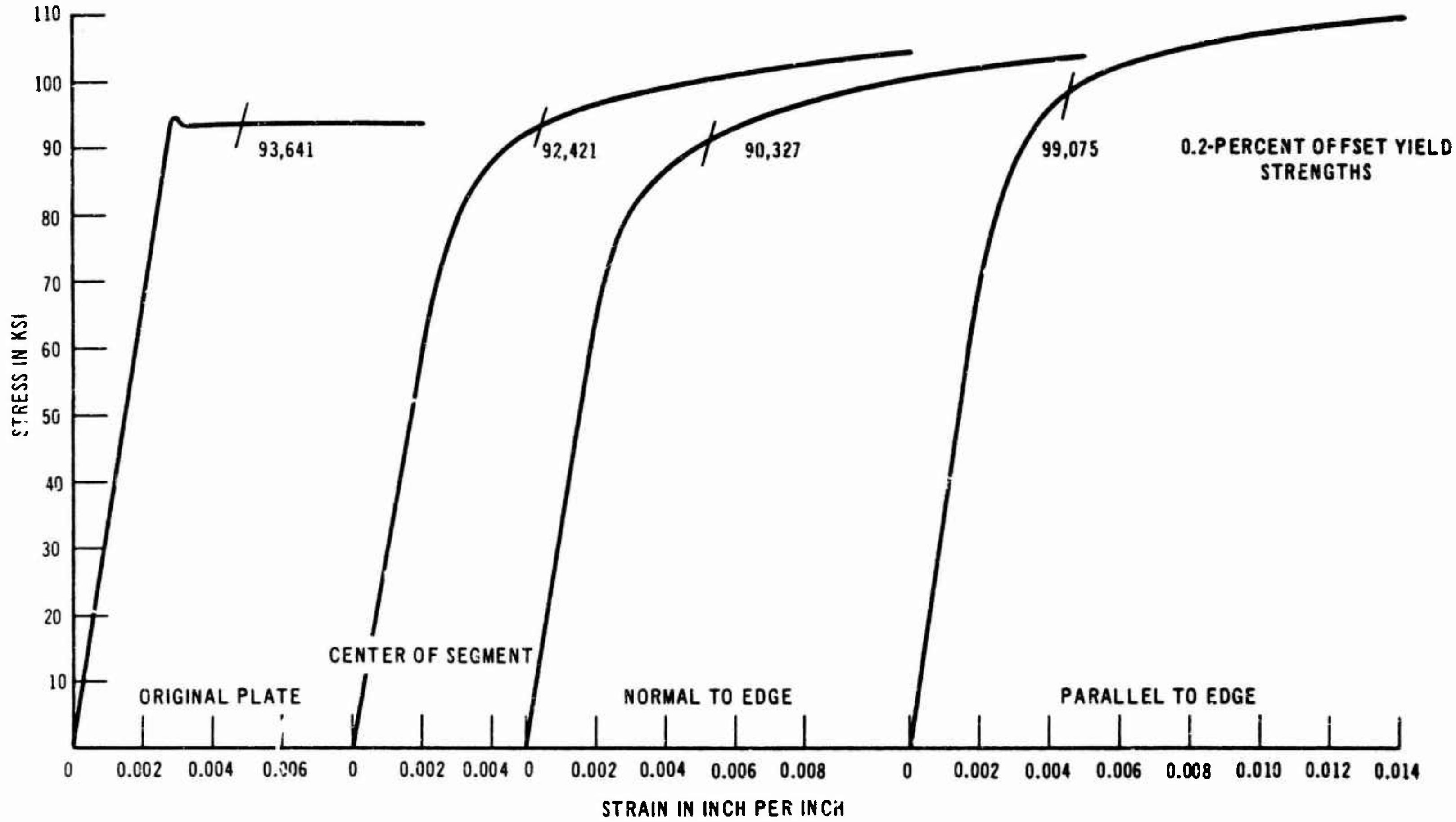

Figure 2 - Typical Stress-Strain Plots for Model 82 from Original Plate and Model after Hydrostatic Testing

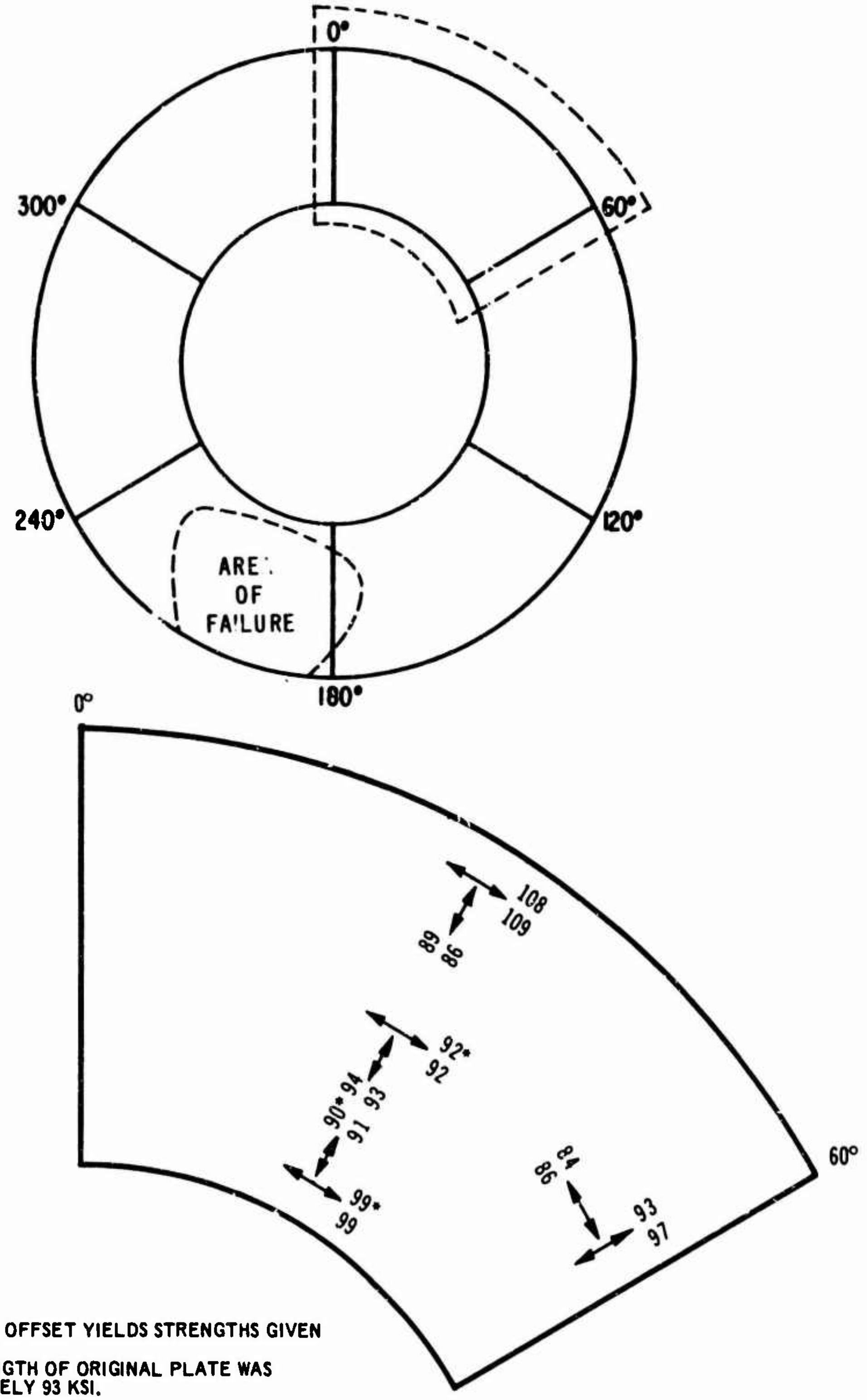

NOTES:

1. 0.2 PERCENT OFFSET YIELDS STRENGTHS GIVEN IN KSI.
2. YIELD STRENGTH OF ORIGINAL PLATE WAS APPROXIMATELY 93 KSI.

*PLOTTED IN FIGURE 9.

Figure 3 - Distribution of Yield Strength from a Typical Formed Segment of Model 82 after Test

Figure 4 - Deviations from Sphericity

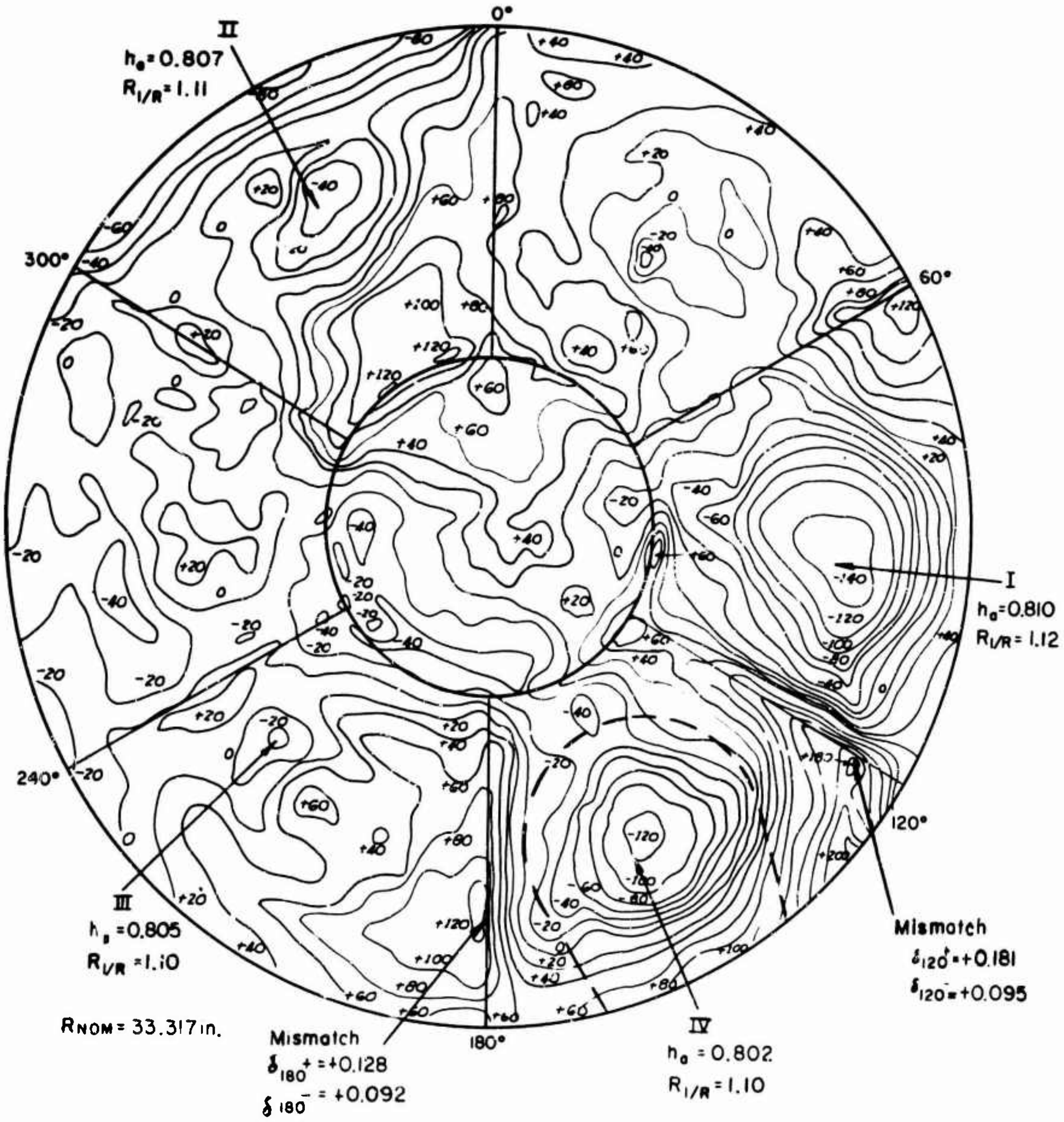

Figure 4a - Model 75

The surface enclosed by the solid circle represents a hemisphere unfolded into a flat surface whose radial scale remains constant. Contours are plotted in mils. Minus contours indicate inward deviations, e.g., -10 indicates distance from center of sphere is R_{nom} - 0.010 in.

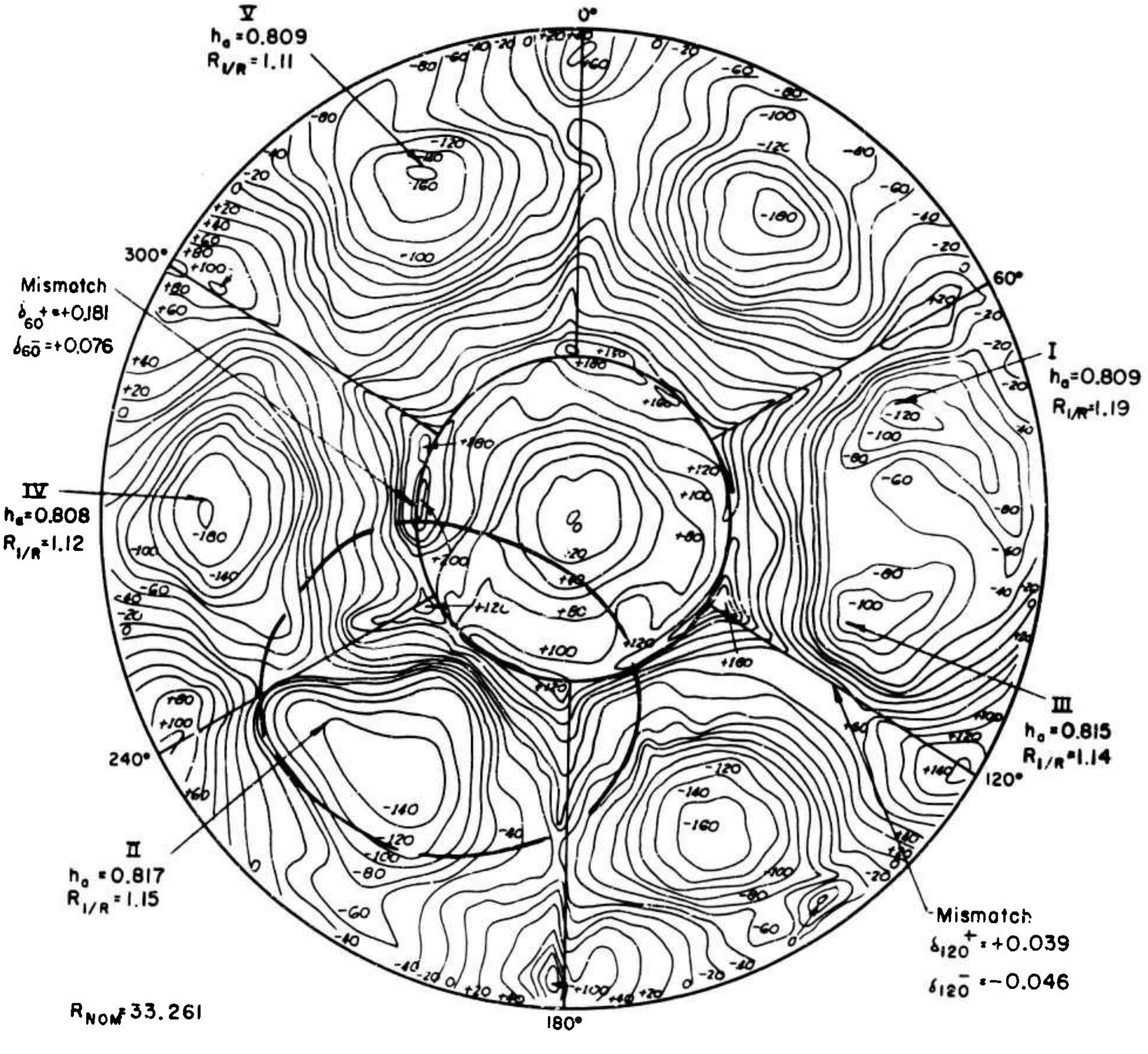

Figure 4b - Model 79

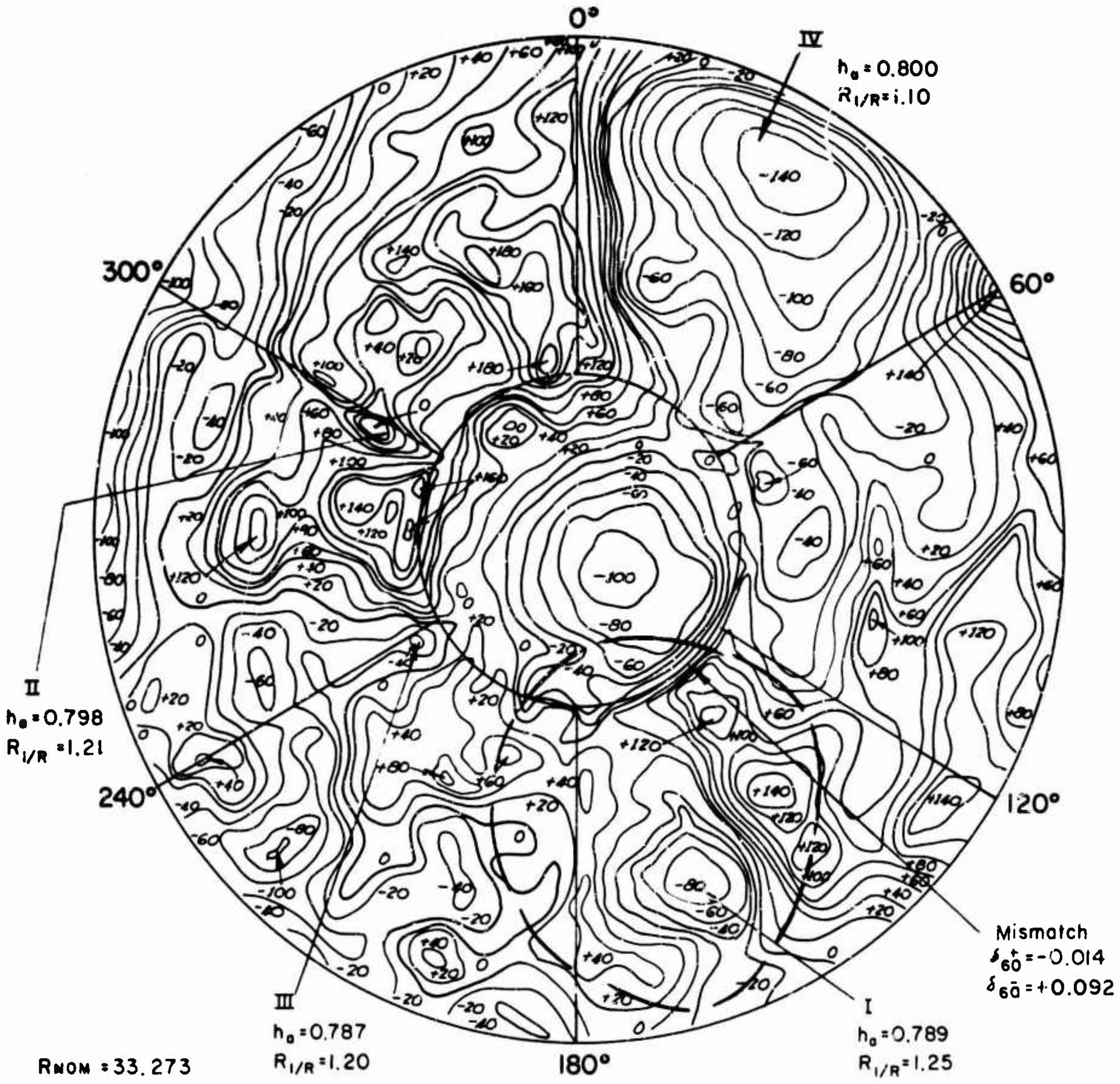

Figure 4c - Model 76

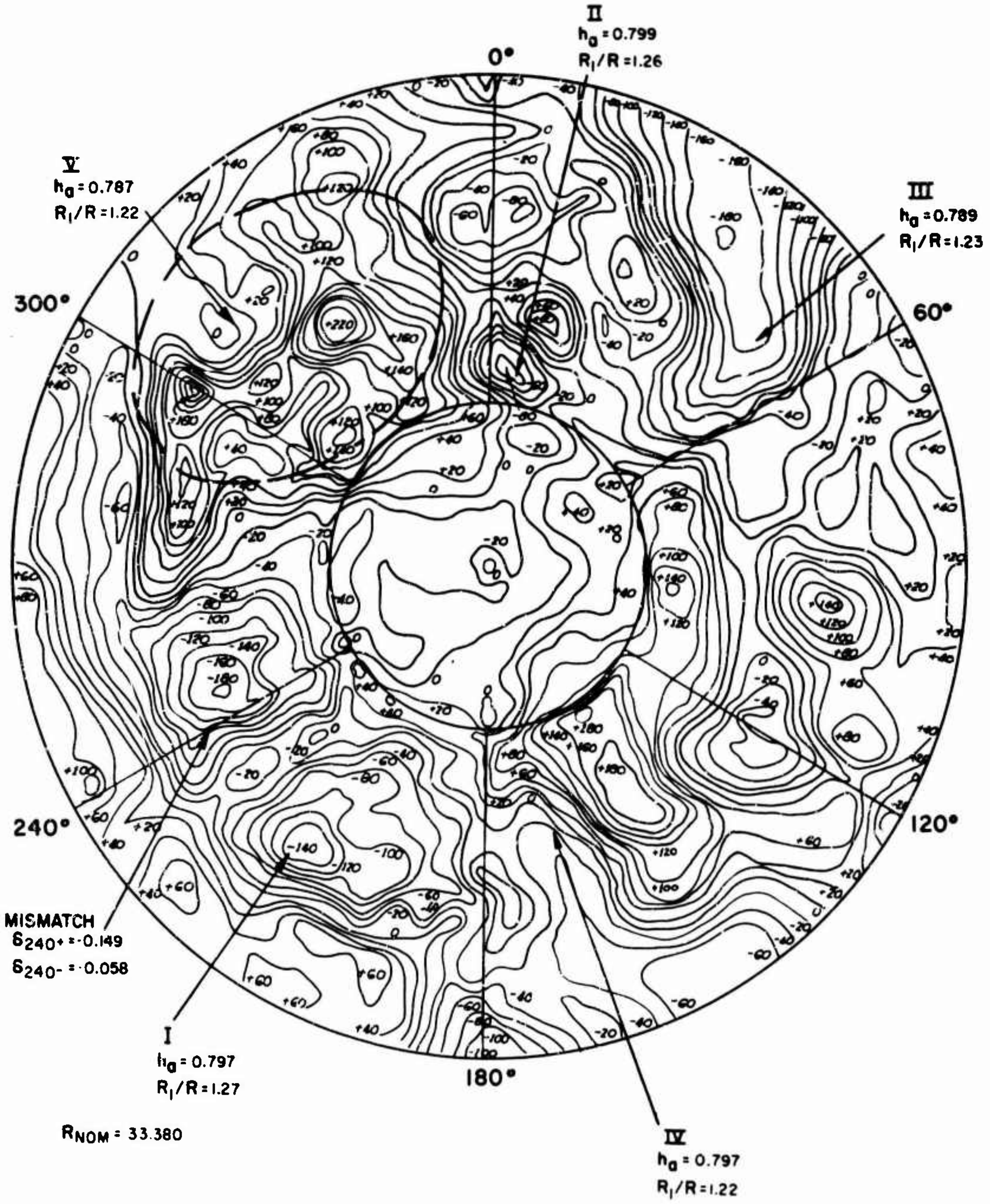

Figure 4d - Model 80

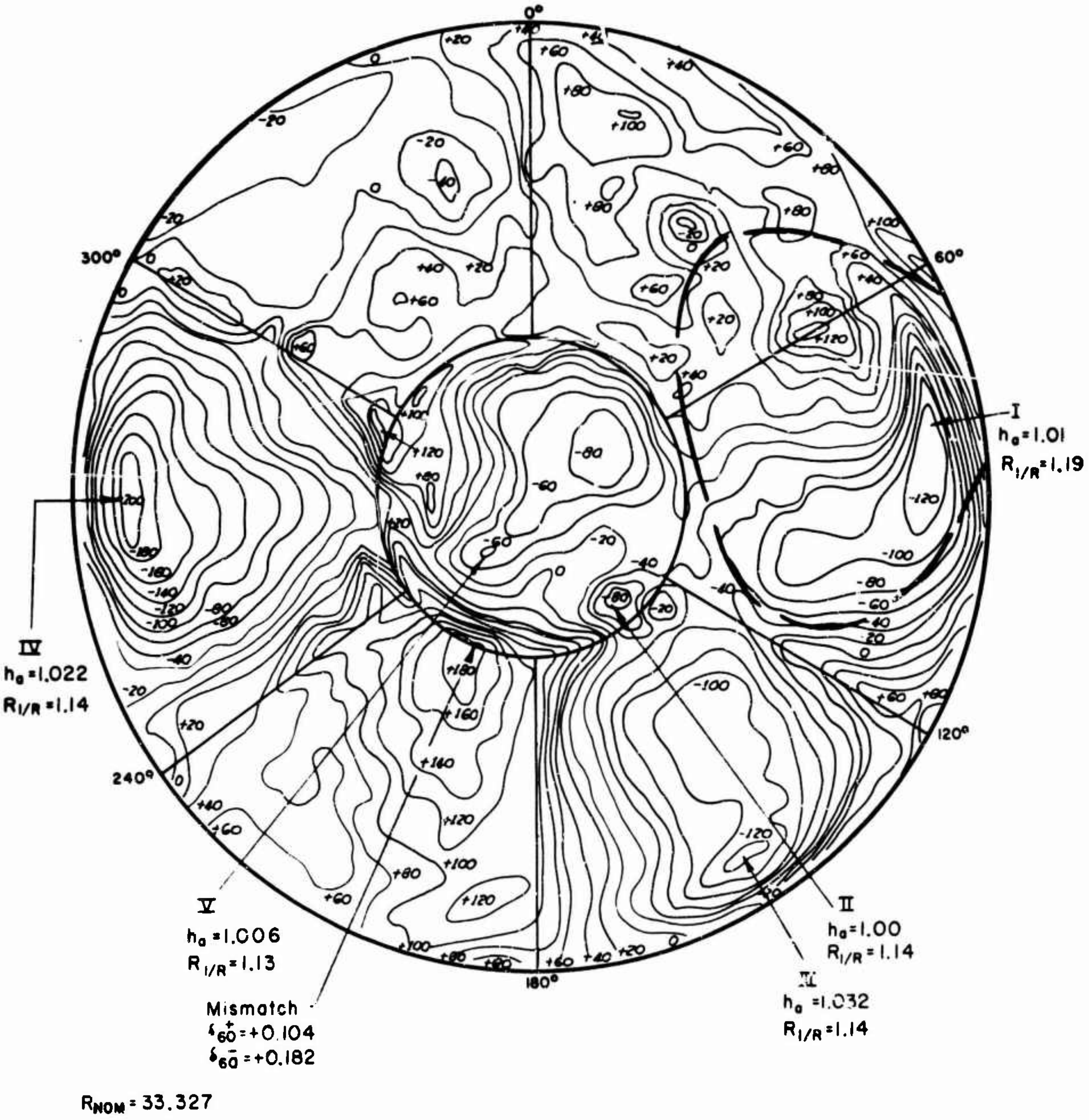

Figure 4e - Model 77

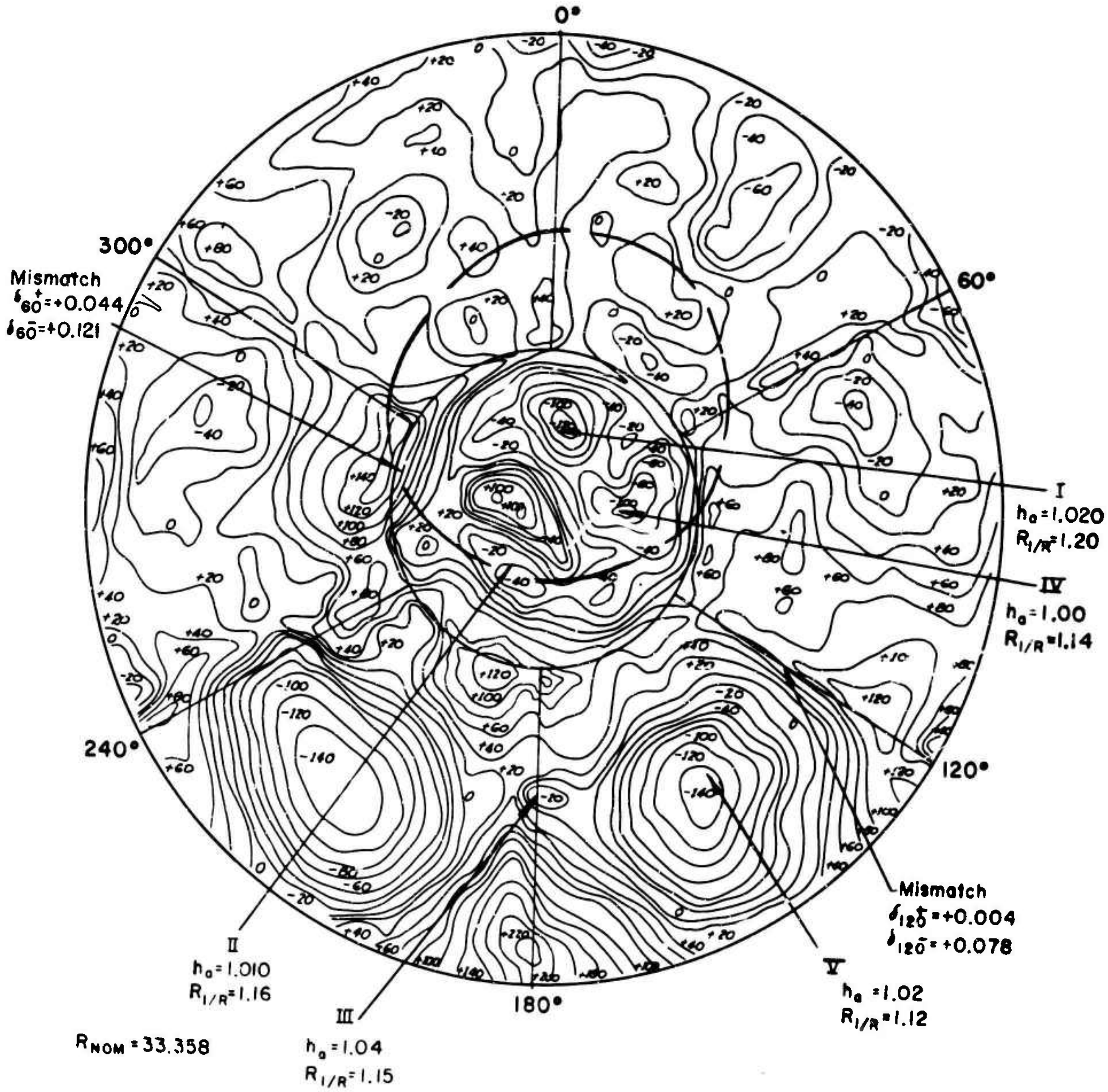

Figure 4f - Model 81

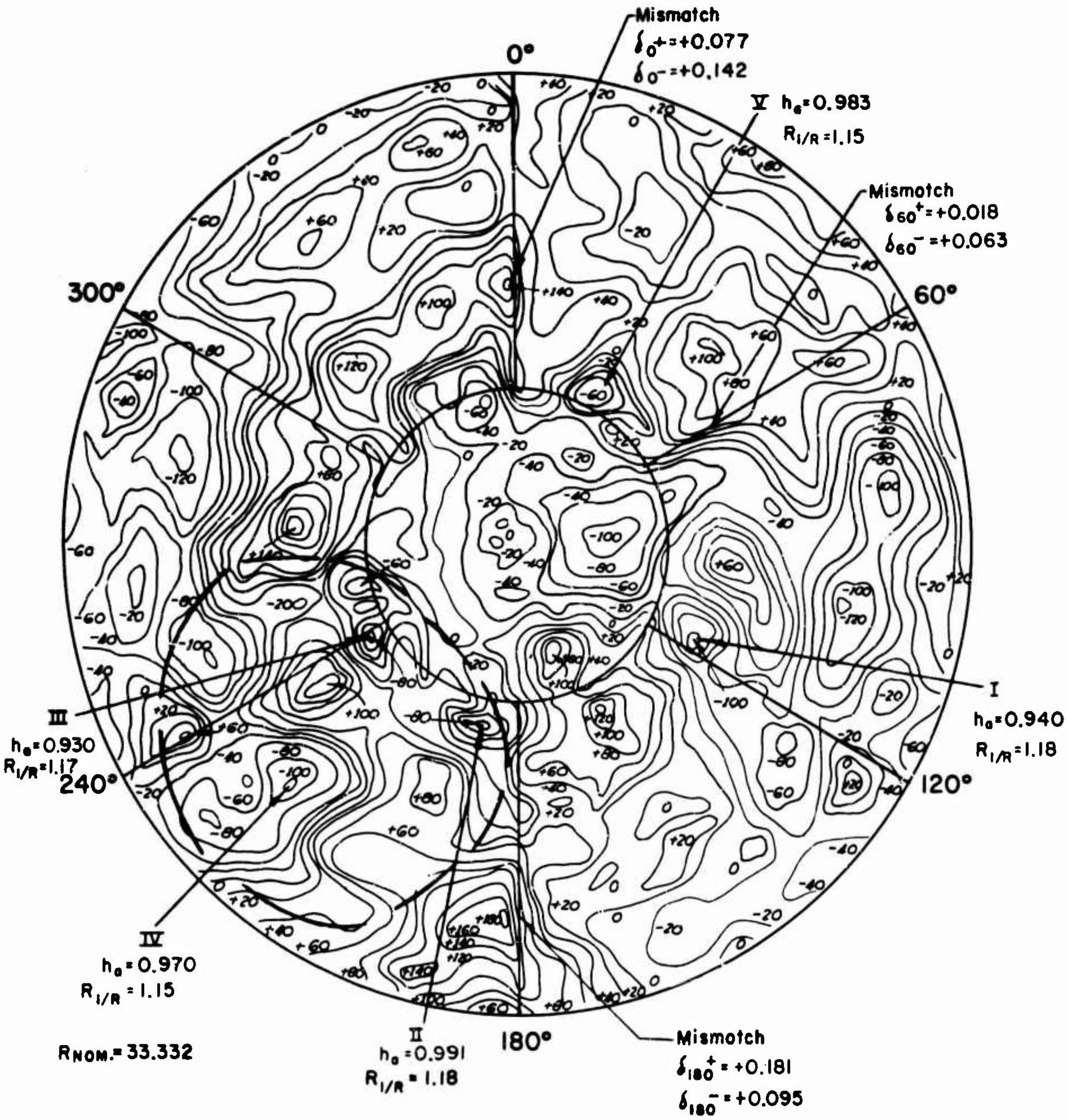

Figure 4g - Model 78

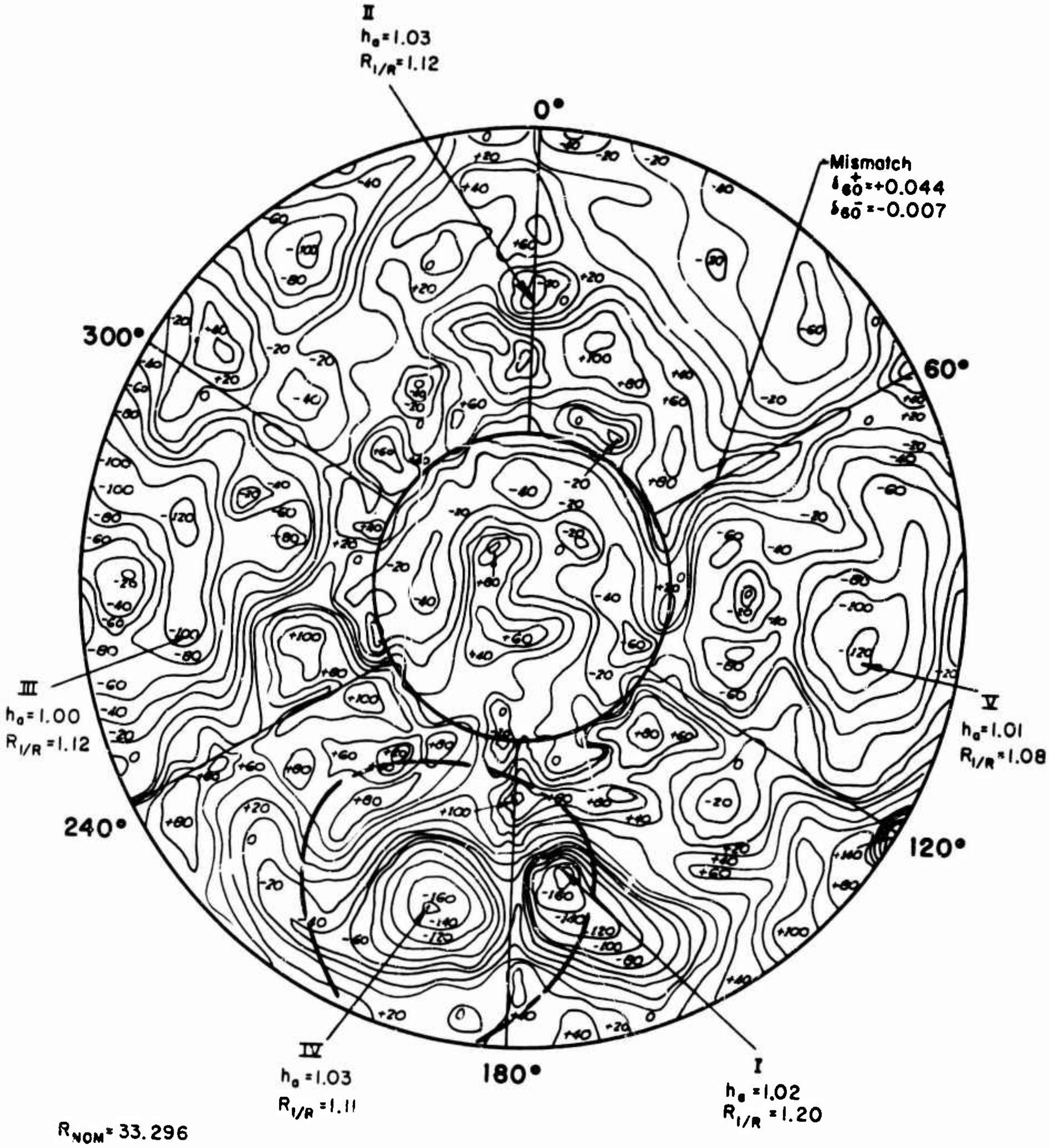

Figure 4h - Model 82

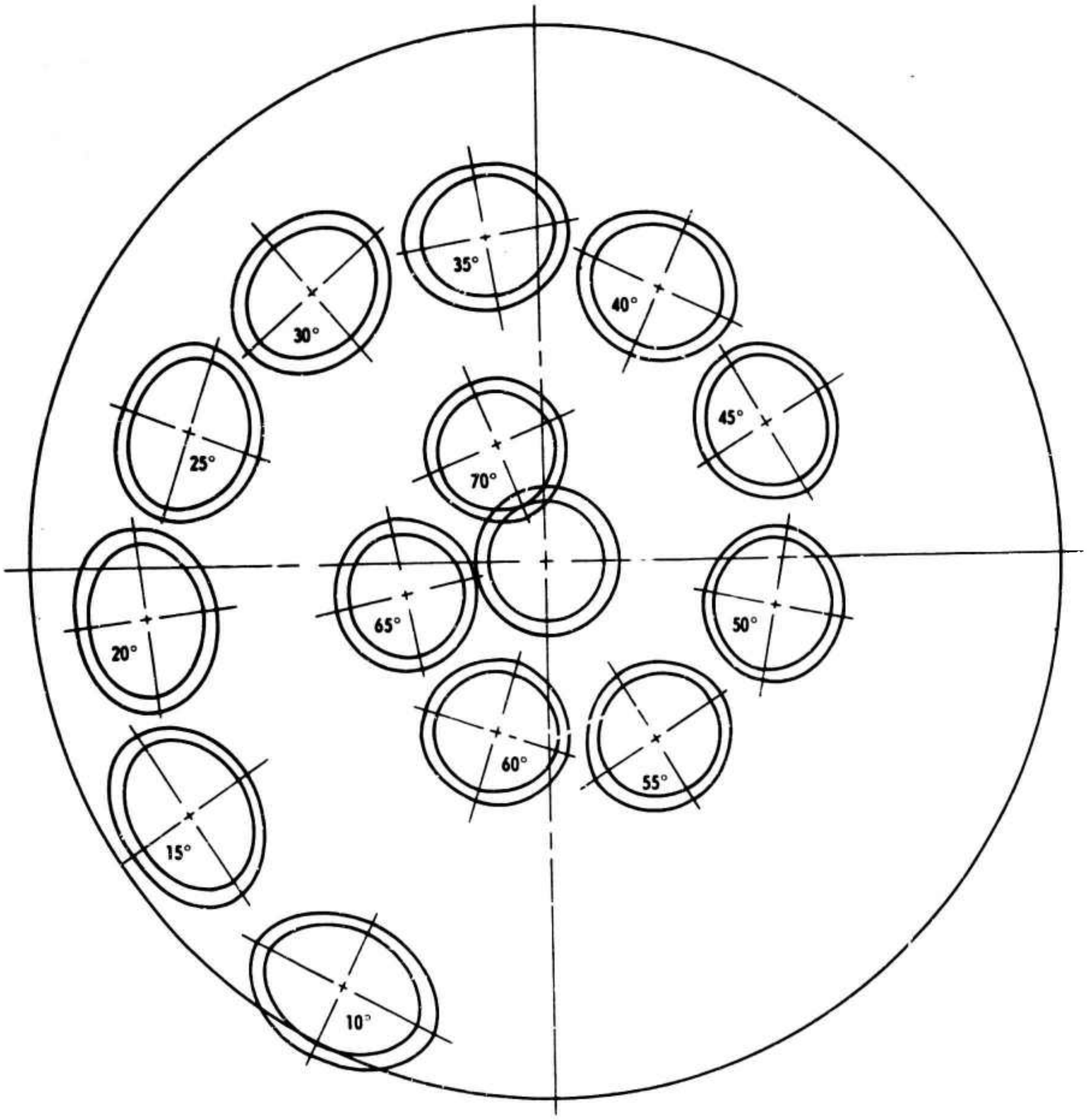

Figure 5 - Arc Length Scales

The surface enclosed by the solid circle shown represents a hemisphere unfolded into a flat surface whose radial scale remains constant.

Mismatch in terms of the deviations from sphericity are also given in Figure 4. It should be noted that in these plots no attempt was made to correct the midsurface shell contours for variations in shell thickness. In addition to the sphericity and mismatch readings, approximately 125 thickness measurements were taken on each model (see Table 2). These measurements indicated that during the pressing operation, the segments tended to thin out at the center and thicken at the edges. Moreover, grinding the welds also caused thickness variations at the edges of the segments. Thus, part of the variations in shell contours is attributable to thickness variations rather than to out-of-roundness of the shell.

The thickness measurements and contour maps were utilized to examine each model for critical local geometry. Each flat spot area was defined by its local thickness h_a and ratio of local to nominal radius R_1/R. A detailed description of the procedure is available in References 6 and 7 and is omitted here. Thickness variations were considered in utilizing the contour maps for out-of-roundness analysis. Although thickness variation influenced the overall shell contours, its effect over a critical arc length could be neglected in most cases.

TEST PROCEDURE

Each model was instrumented with approximately 70 foil-resistance strain gages. Areas for gaging were selected on the basis of flat spot calculations, mismatch data, and thickness readings. In some cases, gages were also placed near the juncture of sphere and cylinder. Strain-gage locations are presented in Figure 6.

The models were statically tested in oil in the 6-ft testing tank at the Model Basin. The test setup is presented in Figure 7. Generally, each test consisted of three pressure runs--the first and second to approximately 70 and 90 percent, respectively, of the collapse pressure and the third to collapse. Pressure was applied in increments, and each increment of pressure was held approximately 5 min. The final increment prior to collapse was less than 2 percent of the collapse pressure.

(Text continued on page 27.)

TABLE 2

Measured Wall Thickness of the Models

Meridional Orientation in Degrees

Circumferential Orientation in Degrees	0^+	15	30	45	60^-	60^+	75	90
0^+	0.800	0.800	0.818	0.815	0.797	0.805	0.810	0.783
15	0.797	0.797	0.800					
30	0.818	0.805	0.795	0.790	0.805	0.813	0.805	
45		0.804	0.807	0.812				
60^-	0.784	0.808	0.794	0.812	0.803	0.816	0.808	
60^+	0.778	0.810	0.765	0.818	0.790			
75		0.805	0.818	0.815				
90	0.819	0.813	0.807	0.792	0.818	0.815	0.809	
105		0.807	0.815	0.817				
120^-	0.786	0.817	0.820	0.817	0.817	0.817	0.805	
120^+	0.823	0.820	0.803	0.780	0.788			
135		0.808	0.800	0.805				
150	0.820	0.809	0.800	0.796	0.811	0.795	0.810	
165	0.800	0.800	0.811	0.803				
180^-	0.810	0.808	0.800	0.810	0.788	0.813	0.813	
180^+	0.817	0.818	0.802	0.787	0.795			
195		0.800	0.805	0.800				
210	0.825	0.812	0.797	0.785	0.803	0.825	0.805	
225		0.805	0.805	0.805				
240^+	0.790	0.800	0.822	0.807	0.795	0.796	0.815	
240^+	0.813	0.824	0.810	0.829	0.810			
255		0.814	0.812	0.817				
270	0.832	0.809	0.803	0.803	0.798	0.798	0.809	
285		0.810	0.803	0.807				
300^-	0.822	0.817	0.814	0.809	0.792	0.790	0.805	
300^+	0.798	0.810	0.794	0.783	0.777			
315		0.810	0.810	0.815				
330	0.825	0.808	0.803	0.787	0.815			
345		0.818	0.818	0.814				
360^-	0.800	0.785	0.825	0.820	0.795			
	$h_{avg.}$ =0.806		$h_{min.}$ =0.765			$h_{max.}$ =0.832		

Model 75

Meridional Orientation in Degrees

Circumferential Orientation in Degrees	0^+	15	30	45	60^-	60^+	75	90
0^+	0.800	0.790	0.830	0.835	0.825	0.800	0.815	805
15		0.818	0.820	0.820				
30	0.830	0.817	0.790	0.800	0.805	0.832	0.813	
45		0.800	0.820	0.815				
60^-	0.810	0.820	0.834	0.830	0.818	0.800	0.815	
60^+	0.817	0.808	0.604	0.818	0.788			
75		0.815	0.810	0.818				
90	0.843	0.810	0.813	0.808	0.820	0.827	0.814	
105		0.805	0.815	0.815				
120^-	0.805	0.815	0.825	0.818	0.805	0.812	0.805	
120^+	0.785	0.815	0.823	0.790	0.805			
135		0.825	0.820	0.817				
150	0.834	0.823	0.820	0.814	0.820	0.814	0.813	
165		0.805	0.817	0.815				
180^-	0.834	0.834	0.830	0.834	0.800	0.826	0.815	
180^+	0.803	0.830	0.842	0.828	0.805			
195		0.815	0.825	0.820				
210	0.837	0.818	0.804	0.818	0.795	0.820	0.815	
225		0.820	0.815	0.817				
240^+	0.823	0.818	0.823	0.825	0.815	0.810	0.813	
240^+	0.820	0.820	0.820	0.823	0.810			
255		0.610	0.815	0.815				
270	0.824	0.810	0.805	0.810	0.815	0.805	0.818	
285		0.809	0.810	0.810				
300^-	0.820	0.800	0.822	0.825	0.792	0.820	0.815	
300^+	0.777	0.793	0.815	0.807	0.790			
315		0.815	0.820	0.820				
330	0.827	0.815	0.810	0.807	0.805	0.817	0.813	
345		0.805	0.807	0.805				
360^-	0.822	0.817	0.830	0.797	0.790			
	$h_{avg.}$ =0.814		$h_{min.}$ =0.777			$h_{max.}$ =0.843		

Model 79

TABLE 2 - (Continued)

Circumferential Orientation in Degrees	Meridional Orientation in Degrees 0^{+}	15	30	45	60^{-}	60^{+}	75	90
0^{+}	0.802	0.795	0.807	0.820	0.785	0.810	0.797	0.765
15		0.800	0.810	0.810				
30	0.817	0.800	0.792	0.787	0.767	0.802	0.800	
45		0.795	0.803	0.795				
60^{-}	0.790	0.790	0.807	0.796	0.777	0.798	0.800	
60^{+}	0.803	0.805	0.822	0.800	0.795			
75		0.805	0.805	0.797				
90	0.820	0.798	0.787	0.792	0.790	0.805	0.800	
105		0.805	0.815	0.806				
120^{-}	0.803	[illegible]	0.817	0.802	0.793	0.802	0.795	
120^{+}	0.798	0.812	0.820	0.804	0.788			
135		0.804	0.797	0.793				
150	0.827	0.794	0.782	0.784	0.773	0.800	0.796	
165		0.795	0.797	0.795				
180^{-}	0.797	0.797	0.803	0.803	0.774	0.807	0.800	
180^{+}	0.810	0.802	0.804	0.802	0.778			
195		0.797	0.790	0.789				
210	0.820	0.802	0.787	0.778	0.790	0.803	0.797	
225		0.810	0.803	0.797				
240^{-}	0.790	0.803	0.812	0.800	0.760	0.807	0.797	
240^{+}	0.802	0.797	0.812	0.804	0.795			
255		0.787	0.792	0.794				
270	0.810	0.796	0.783	0.793	0.797	0.813	0.798	
285		0.796	0.795	0.795				
300^{-}	0.797	0.807	0.814	0.812	0.803	0.813	0.805	
300^{+}	0.797	0.793	0.808	0.805	0.773			
315		0.785	0.793	0.815				
330	0.807	0.790	[illegible]	0.787	0.792			
345		0.792	0.793	0.800				
360^{-}	0.796	0.790	0.807	0.807	0.775			
	$h_{avg.}$ =0.798		$h_{min.}$ =0.760			$h_{max.}$ =0.827		

Model 76

Circumferential Orientation in Degrees	Meridional Orientation in Degrees 0^{+}	15	30	45	60^{-}	60^{+}	75	90
0^{+}	0.783	0.795	0.770	0.765	0.805	0.743	0.797	0.750
15		0.785	0.795	0.793				
30	0.820	0.800	0.782	0.787	0.773	0.800	0.793	
45		0.800	0.790	0.798				
60^{-}	0.765	0.785	0.765	0.822	0.745	0.775	0.793	
60^{+}	0.805	0.803	0.790	0.803	0.830			
75		0.800	0.800	0.783				
90	0.823	0.795	0.783	0.787	0.715	0.778	0.793	
105		0.800	0.800	0.796				
120^{-}	0.773	0.845	0.800	0.787	0.755	0.775	0.797	
120^{+}	0.783	0.855	0.810	0.773	0.850			
135		0.800	0.790	0.795				
150	0.825	0.790	0.787	0.787	0.740	0.787	0.793	
165		0.805	0.805	0.805				
180^{-}	0.765	0.755	0.785	0.795	0.835	0.770	0.797	
180^{+}	0.793	0.795	0.815	0.810	0.702			
195		0.792	0.800	0.800				
210	0.816	0.795	0.792	0.790	0.763	0.778	0.793	
225		0.797	0.797	0.797				
240^{-}	0.777	0.765	0.787	0.787	0.780	0.777	0.795	
240^{+}	0.750	0.765	0.787	0.790	0.850			
255		0.805	0.802	0.800				
270	0.827	0.790	0.787	0.785	0.820	0.777	0.792	
285		0.805	0.790	0.793				
300^{-}	0.790	0.795	0.770	0.780	0.770	0.772	0.792	
300^{+}	0.785	0.787	0.780	0.790	0.775			
315		0.793	0.790	0.800				
330	0.828	0.792	0.768	0.780	0.743	0.775	0.792	
345		0.803	0.800	0.793				
360^{-}	0.845	0.775	0.728	0.720	0.750			
	$h_{avg.}$ =0.789		$h_{min.}$ =0.702			$h_{max.}$ =0.855		

Model 80

TABLE 2 - (Continued)

Meridional Orientation in Degrees

Circumferential Orientation in Degrees	0^{+}	15	30	45	60^{-}	60^{+}	75	90
0^{+}	1.000	1.025	1.000	1.020	0.977	0.978	0.987	0.990
15		1.003	1.002	1.004				
30	1.050	1.010	1.000	0.985	0.992	0.978	1.010	
45		1.017	1.012	1.008				
60^{-}	1.004	1.005	0.970	0.963	1.030	1.025	1.013	
60^{+}	1.000	1.005	1.009	1.020	1.005			
75		1.010	1.012	1.022				
90	1.025	1.010	1.010	1.012	1.025	1.033	1.003	
105		1.010	1.010	1.015				
120^{-}	0.980	0.958	0 995	0.997	0.993	1.020	1.010	
120^{+}	1.030	1.018	1.018	1.015	0.990			
135		1.015	1.015	1.012				
150	1.055	1.020	1.008	0.995	0.985	1.015	1.008	
165		1.015	1.015	1.015				
180^{-}	0.980	1.000	1.015	1.020	0.975	1.015	1.005	
180^{+}	1.013	1.005	1.015	1.018	0.993			
195		1.005	0.998	1.003				
210	1.025	1.012	0.990	0.988	0.983	1.007	1.005	
225		1.018	1.005	1.008				
240^{-}	0.993	1.010	1.010	0.970	0.970	1.005	1.008	
240^{+}	1.020	1.008	1.018	1.015	0.975			
255		1.010	1.007	1.005				
270	1.035	1.015	1.000	0.983	1.000	1.025	1.005	
285		1.008	1.012	1.014				
300^{-}	1.010	1.010	1.015	1.005	0.990	1.010	1.005	
300^{+}	1.015	1.028	1.040	1.035	0.998			
315		1.012	1.005	1.010				
330	1.012	1.003	0.997	1.000	1.022	0.975	0.997	
345		1.005	1.008	1.010				
360^{-}	0.993	1.008	0.993	1.009	0.987			

$h_{avg.}$ =1.006 $h_{min.}$ =0.970 $h_{max.}$ =1.055

Model 77

Meridional Orientation in Degrees

Circumferential Orientation in Degrees	0^{+}	15	30	45	60^{-}	60^{+}	75	90
0^{+}	1.015	1.020	1.035	1.040	1.030	1.030	1.025	0.985
15		1.015	1.000	1.015				
30	1.050	1.020	1.000	1.000	1.015	1.005	1.005	
45		1.020	1.023	1.125				
60^{-}	1.025	1.005	1.035	1.025	1.025	1.025	1.001	
60^{+}	1.020	1.015	1.030	1.030	1.020			
75		1.020	1.000	1.025				
90	1.055	1.010	1.000	1.010	0.995	1.110	1.000	
105		1.115	1.110	1.030				
120^{-}	0.980	1.025	1.055	1.045	0.995	1.010	1.000	
120^{+}	1.035	1.035	1.045	1.045	1.000			
135		1.025	1.015	1.025				
150	1.055	1.025	1.015	0.995	1.010	1.025	1.010	
165		1.015	1.020	1.025				
180^{-}	1.015	1.055	1.025	1.055	1.025	1.020	1.015	
180^{+}	1.015	1.025	1.040	1.040	0.995			
195		1.020	1.010	1.020				
210	1.050	1.015	1.010	1.010	1.020	1.040	1.015	
225		1.020	1.000	1.015				
240^{-}	1.035	1.030	1.010	1.030	1.015	1.035	1.015	
240^{+}	1.015	1.030	1.030	1.020	1.015			
255		1.025	1.010	1.020				
270	1.050	1.010	0.990	1.005	1.010	1.025	1.010	
285		1.020	1.015	1.025				
300^{-}	1.035	1.035	1.055	1.030	1.000	1.025	1.015	
300^{+}	1.025	1.030	1.040	1.040	0.985			
315		1.015	1.010	1.025				
330	1.050	1.015	1.015	1.020	1.015	1.030	1.010	
345		1.020	1.015	1.020				
360^{-}	0.985	1.000	1.030	1.045	1.015			

$h_{avg.}$ =1.022 $h_{min.}$ =0.980 $h_{max.}$ =1.055

Model 81

TABLE 2 - (Continued)

	Meridional Orientation in Degrees							
Circumferential Orientation in Degrees	0^+	15	30	45	60^-	60^+	75	90
0^+	0.985	1.010	1.000	1.000	0.975	0.975	1.010	0.982
15		1.018	1.015	1.020				
30	1.040	1.015	1.000	1.020	0.900	1.000	1.000	
45		1.010	1.020	1.015				
60^-	1.010	1.015	0.990	1.010	0.980	1.005	1.020	
60^+	0.895	1.015	0.985	1.010	0.900			
75		1.015	1.005	1.015				
90	1.030	1.005	0.988	1.000	0.993	1.030	1.010	
105		1.013	1.000	1.010				
120^-	0.995	1.010	0.970	0.980	0.910	0.950	1.000	
120^+	0.890	1.000	0.975	0.860	0.950			
135		0.892	1.010	1.013				
150	1.040	1.010	0.975	0.990	0.968	0.958	1.012	
165		1.020	1.010	1.003				
180^-	0.990	0.995	0.990	0.971	0.978	0.980	1.000	
180^+	1.000	0.965	0.970	0.970	0.985			
195		1.020	1.013	1.018				
210	0.940	1.005	0.990	0.970	0.980	1.008	1.010	
225		1.015	1.010	1.015				
240^-	1.005	1.015	0.990	0.970	0.989	0.968	1.015	
240^+	0.990	0.990	0.975	0.950	0.920			
255		1.015	1.015	1.015				
270	0.945	1.005	0.997	0.998	0.985	1.005	1.015	
285		1.005	1.010	1.010				
300^-	1.000	0.960	1.015	0.990	0.960	1.005	1.010	
300^+	0.970	0.970	1.010	0.988	0.970			
315		1.020	1.018	1.025				
330	1.040	1.020	1.008	1.000	0.975	0.995	1.003	
345		1.005	1.015	1.010				
360^-	1.000	1.010	1.018	0.985	0.875			
	$h_{avg.}$ =0.992		$h_{min.}$ =0.860			$h_{max.}$ =1.040		

Model 78

	Meridional Orientation in Degrees							
Circumferential Orientation in Degrees	0^+	15	30	45	60^-	60^+	75	90
0^+	0.990	1.005	1.035	1.030	1.025	0.988	1.010	0.998
15		1.020	1.012	1.005				
30	1.045	1.020	1.005	0.995		1.008	1.005	
45		1.020	1.005	1.010				
60^-	0.995	1.012	1.018	1.035	0.985	1.015	0.990	
60^+	1.010	1.025	0.985	1.040	0.990			
75		1.015	1.015	1.030				
90	1.020	1.010	1.015	0.998	1.005	1.010	1.020	
105		1.005	1.010	1.022				
120^-	1.010	1.015	1.035	1.020	0.980	0.950	1.000	
120^+	1.025	1.005	1.055	1.055	1.030			
135		1.020	1.020	1.020				
150	1.040	1.020	1.000	0.990	1.030	1.020	1.015	
165		1.035	1.020	1.030				
180^-	1.020	1.030	1.035	1.038	0.990	1.010	1.015	
180^+	1.020	0.955	0.945	1.025	1.005			
195		1.030	1.020	1.025				
210	1.040	1.010	1.000	0.995	1.015	1.030	1.018	
225		1.020	1.000	1.000				
240^-	0.985	1.000	1.030	1.030	0.980	1.005	1.010	
240^+	0.955	1.000	1.010	1.030	0.990			
255		1.005	1.005	1.005				
270	1.020	1.000	0.990	1.000	1.008	1.005	1.008	
285		1.008	1.000	1.025				
300^-	0.980	1.020	1.025	1.040	1.000	0.970	1.008	
300^+	1.030	1.028	1.045	1.040	0.990			
315		1.025	1.010	1.022				
330	1.038	1.015	1.000	1.005	1.010	0.970	1.010	
345		1.010	1.025	1.020				
360^-	1.030	0.995	1.020	1.025	0.968			
	$h_{avg.}$ =1.012		$h_{min.}$ =0.945			$h_{max.}$ =1.045		

Model 82

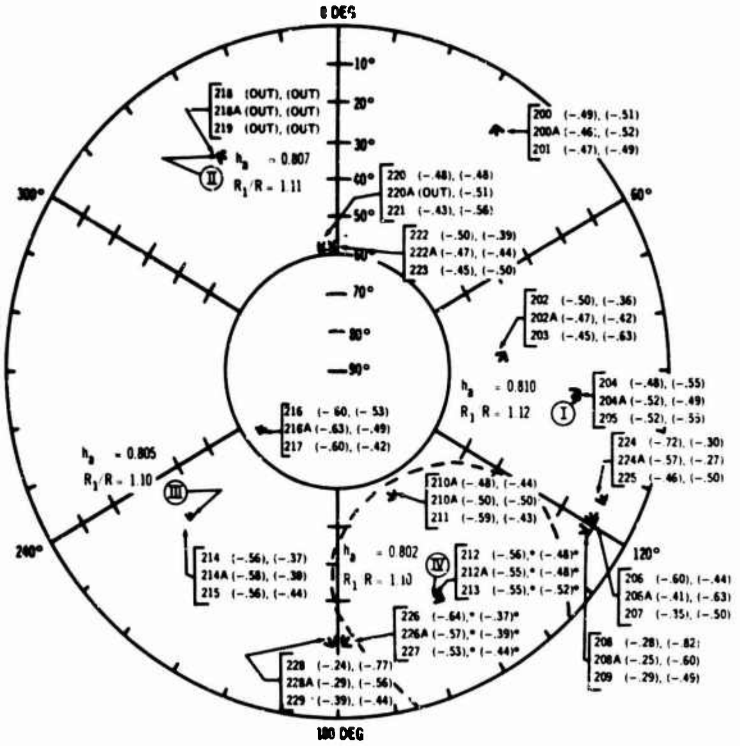

Figure 6a - Model 75

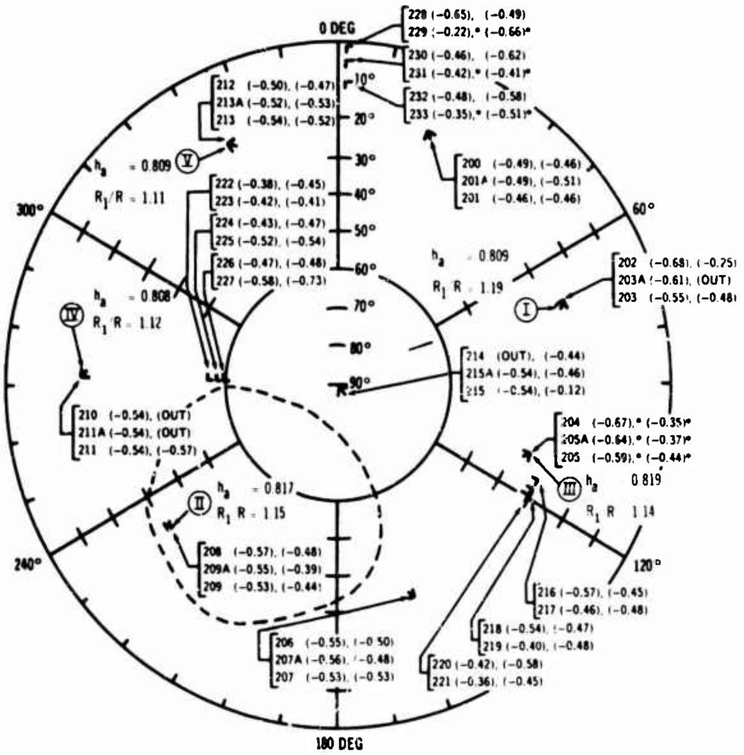

Figure 6b - Model 79

Figure 6 - Strain-Gage Locations and Strain Sensitivities

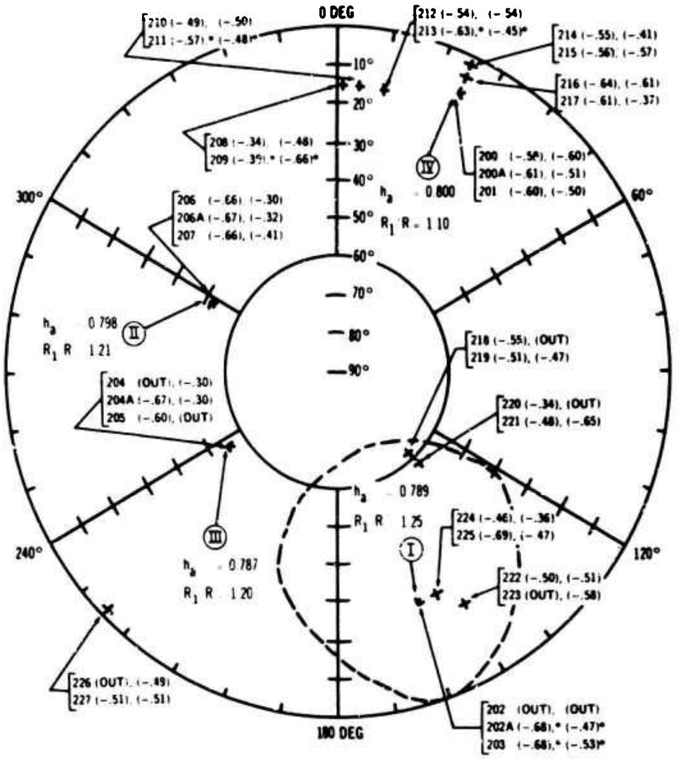

Figure 6c - Model 76

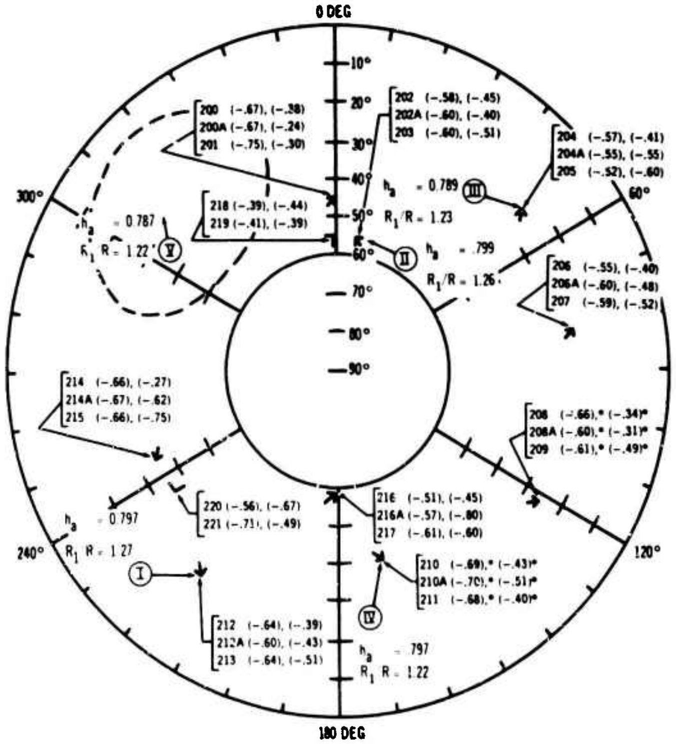

Figure 6d - Model 80

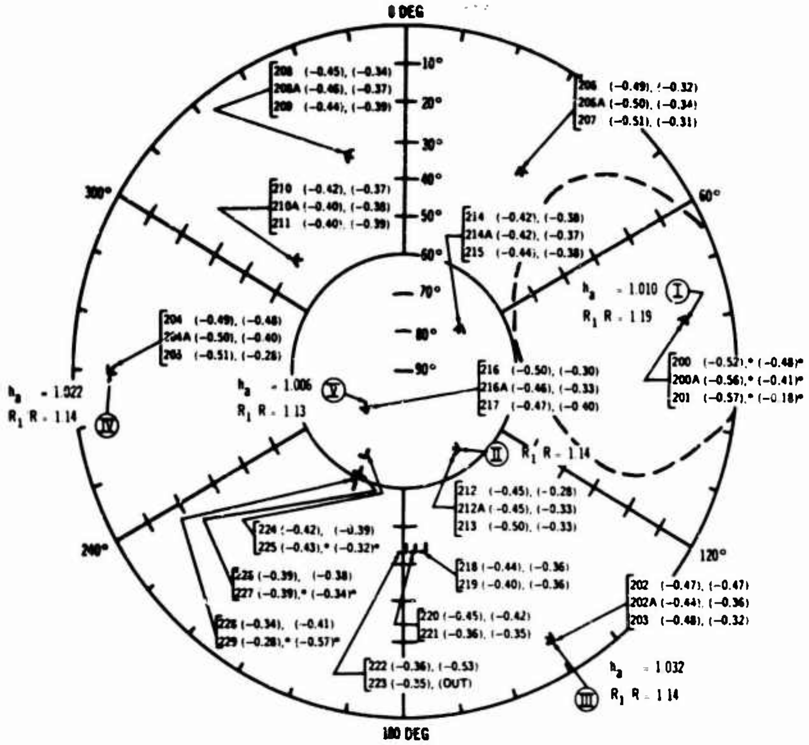

Figure 6e - Model 77

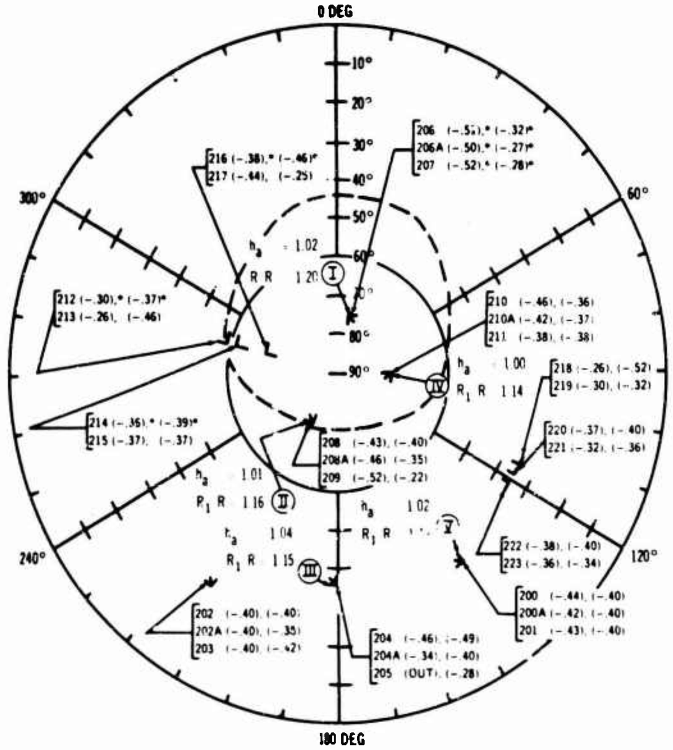

Figure 6f - Model 81

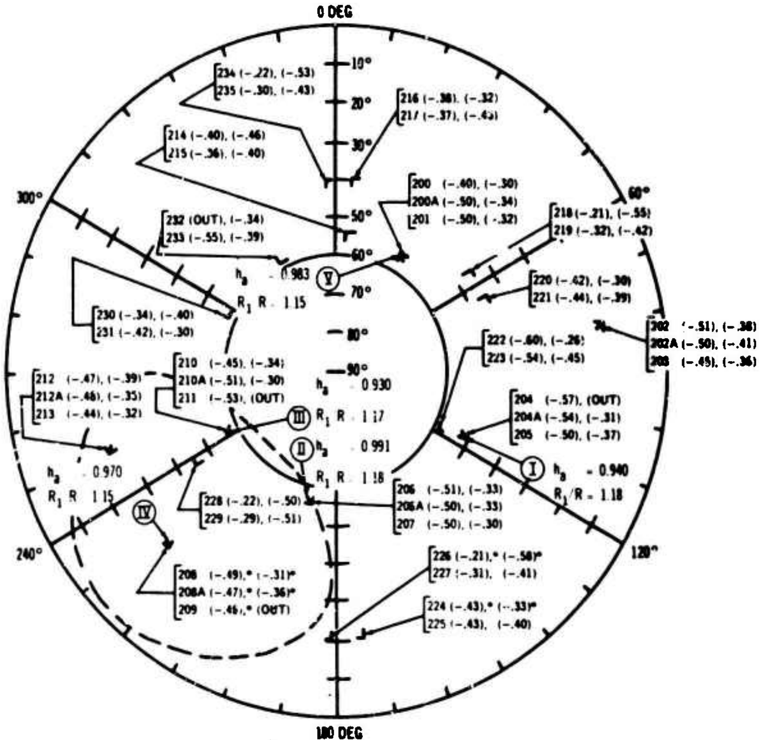

Figure 6g - Model 78

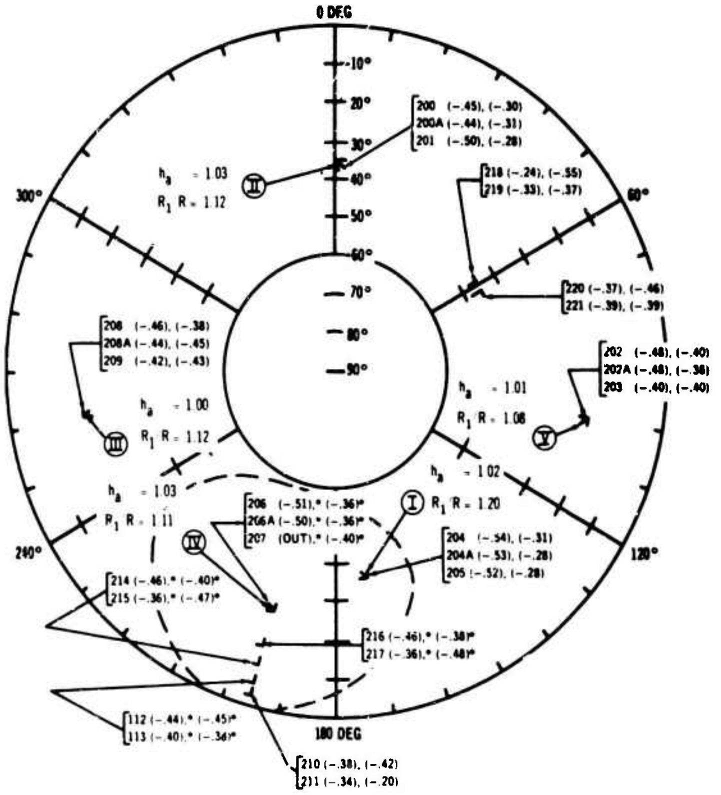

Figure 6h - Model 82

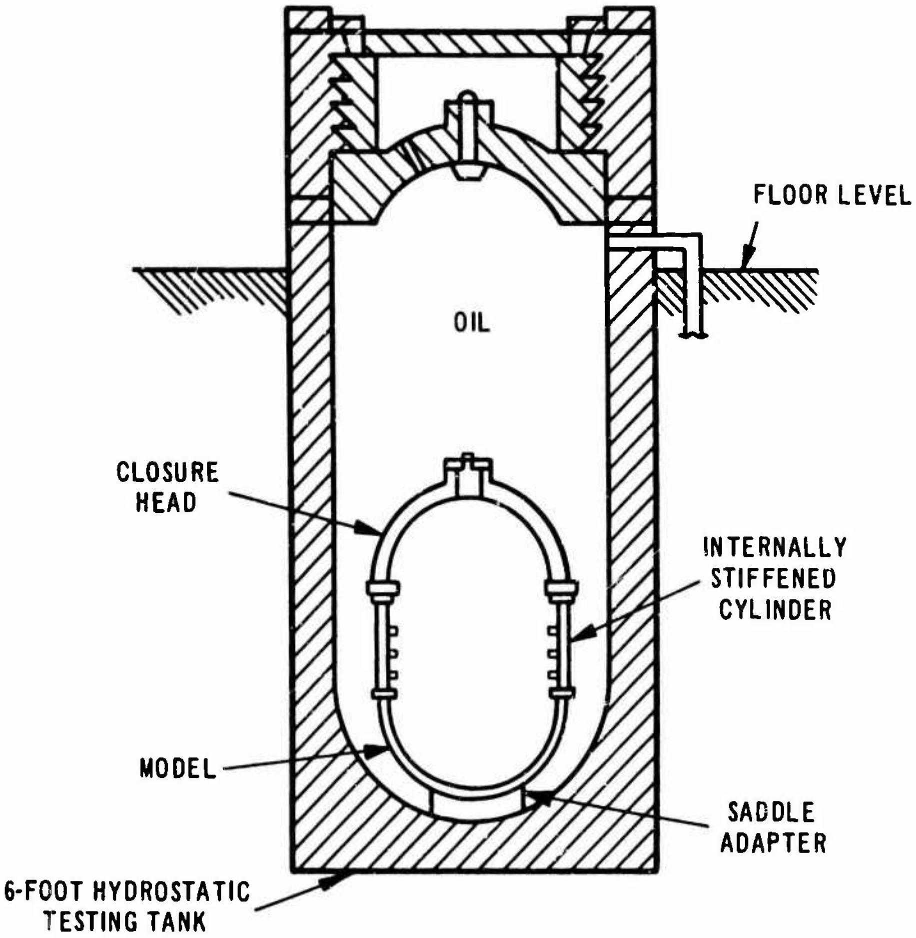

Figure 7 - Test Setup

RESULTS AND DISCUSSION

Experimental collapse pressures for each model are shown in Table 3. Strain sensitivities are shown in Figure 6, and typical pressure-strain plots are given in Figure 8. Figure 9 shows the models after collapse.

Nondimensional plots of experimental results for the eight models are presented in Figure 10; the abscissa is the ratio of elastic buckling pressure P_3' to the yield pressure P_y', and the ordinate is the ratio of the experimental collapse pressure P_c to P_y'. It should be noted that local geometry in the area of failure was used to calculate P_3' and P_y', which are defined by the expressions

$$P_3' = 0.84E\left(\frac{h_a}{R_{10}}\right)^2 \text{ for } \nu = 0.3 \qquad [1]$$

$$P_y' = \frac{2\,\sigma_y\,h_a\,R_{1m}}{(R_{10})^2} \qquad [2]$$

where h_a is the average thickness at the flat spot,

R_{10} is the local outside radius,

R_{1m} is the local midsurface radius,

E is Young's modulus, and

σ_y is the yield strength.

Results of Reference 6 have been included for comparison. It can be observed that the present results are in excellent agreement with previous trends for both as-fabricated and stress-relieved models. The difference between the yield line and the lower bound for the stress-relieved models is attributed to the effect of secondary moments. It appears that this effect becomes negligible as the shells attain margins of stability (P_3'/P_y') of three and greater. The difference between the lower bound trends for stress-relieved and as-fabricated models is attributed to the presence of residual stresses. As the shells become more stable, the effect of residual stresses on collapse strength decreases. It is significant to note the collapse pressures obtained in these eight tests could be predicted within 10 percent by utilizing the imperfection analysis and simply extrapolating test results of Reference 6.

(Text continued on page 34.)

Figure 8 - Typical Pressure-Strain Plots

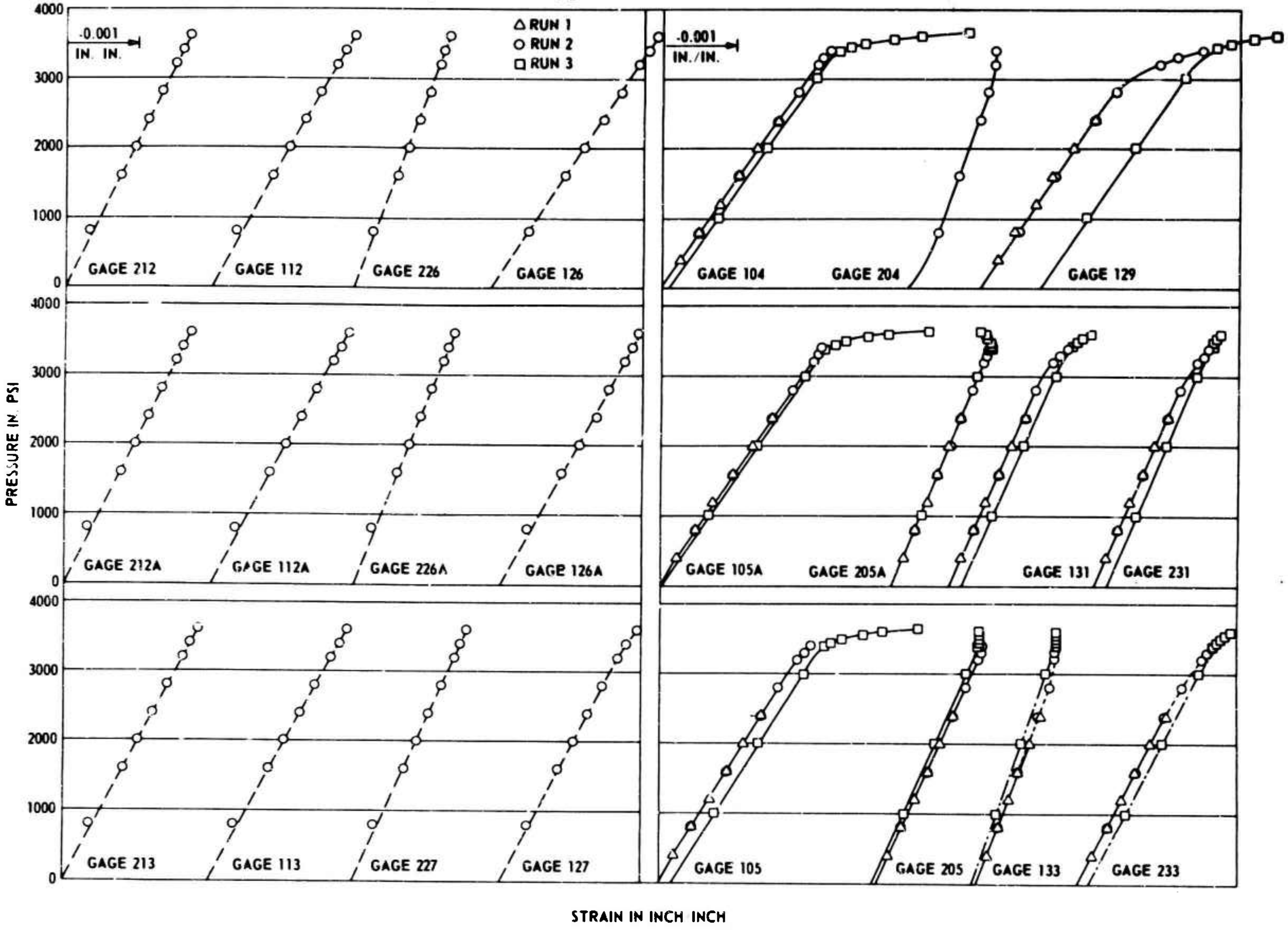

Figure 8a - Model 75

Figure 8b - Model 79

Figure 8 (Continued)

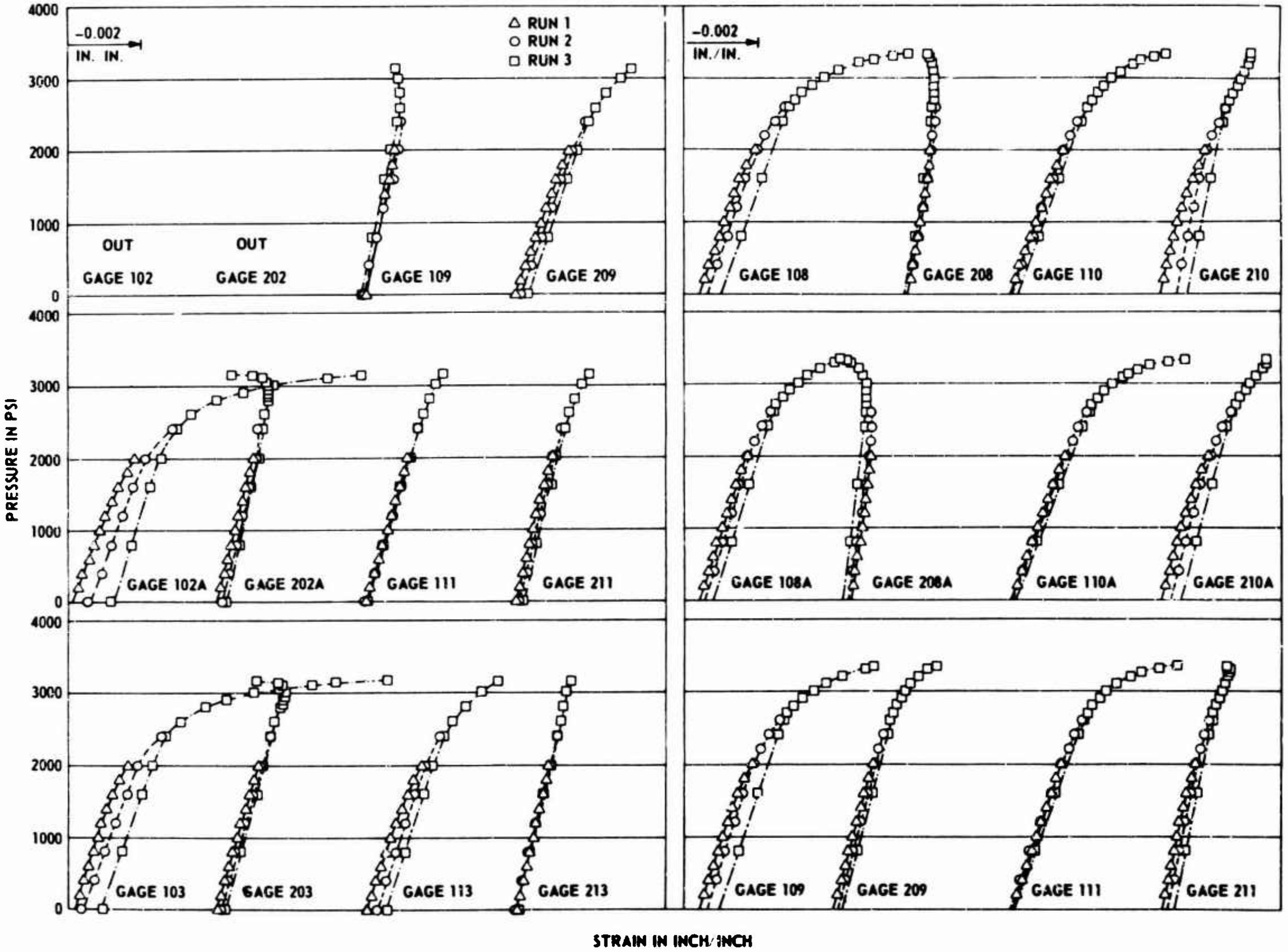

Figure 8c - Model 76

Figure 8d - Model 80

Figure 8 (Continued)

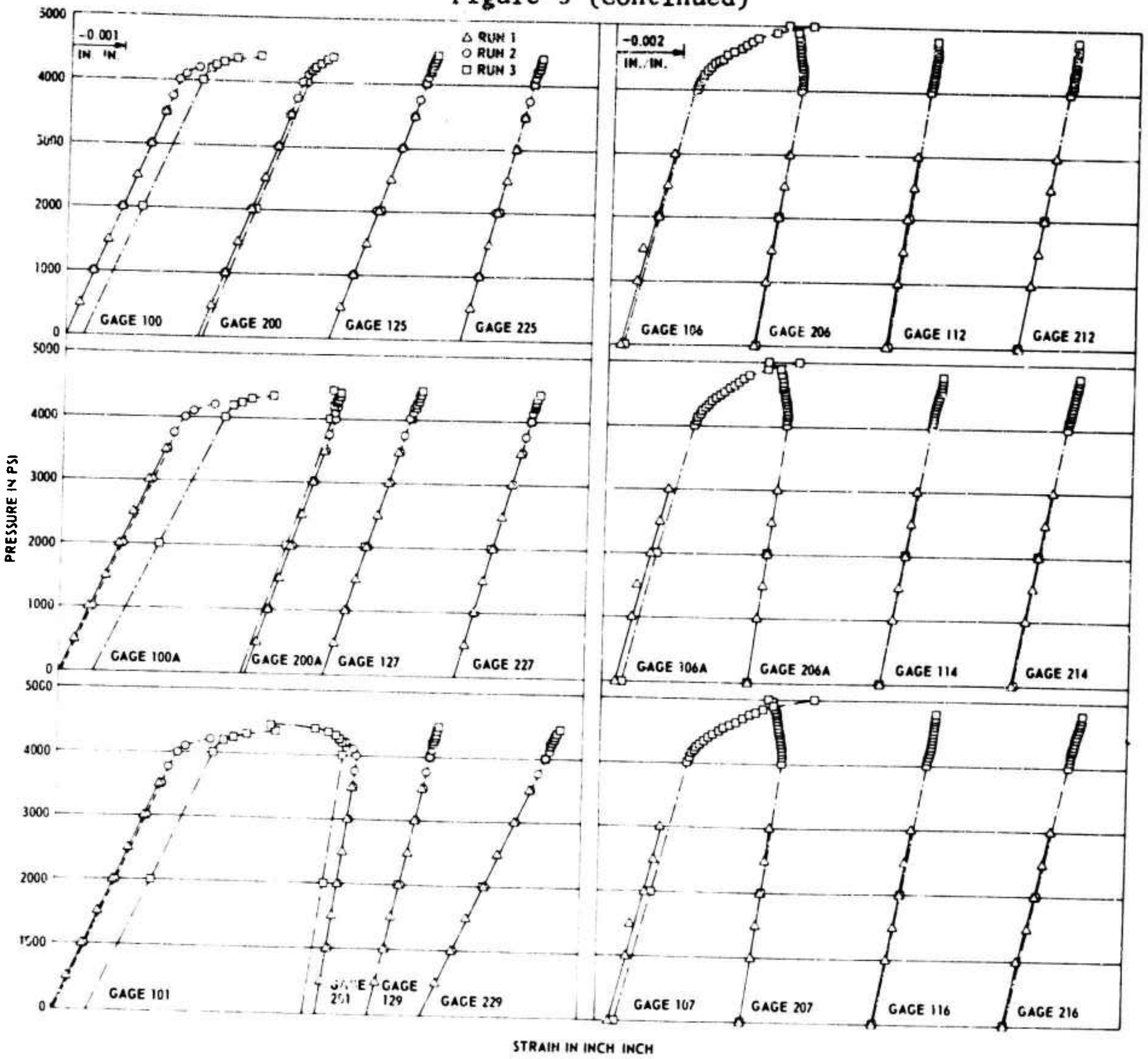

Figure 8e - Model 77

Figure 8f - Model 81

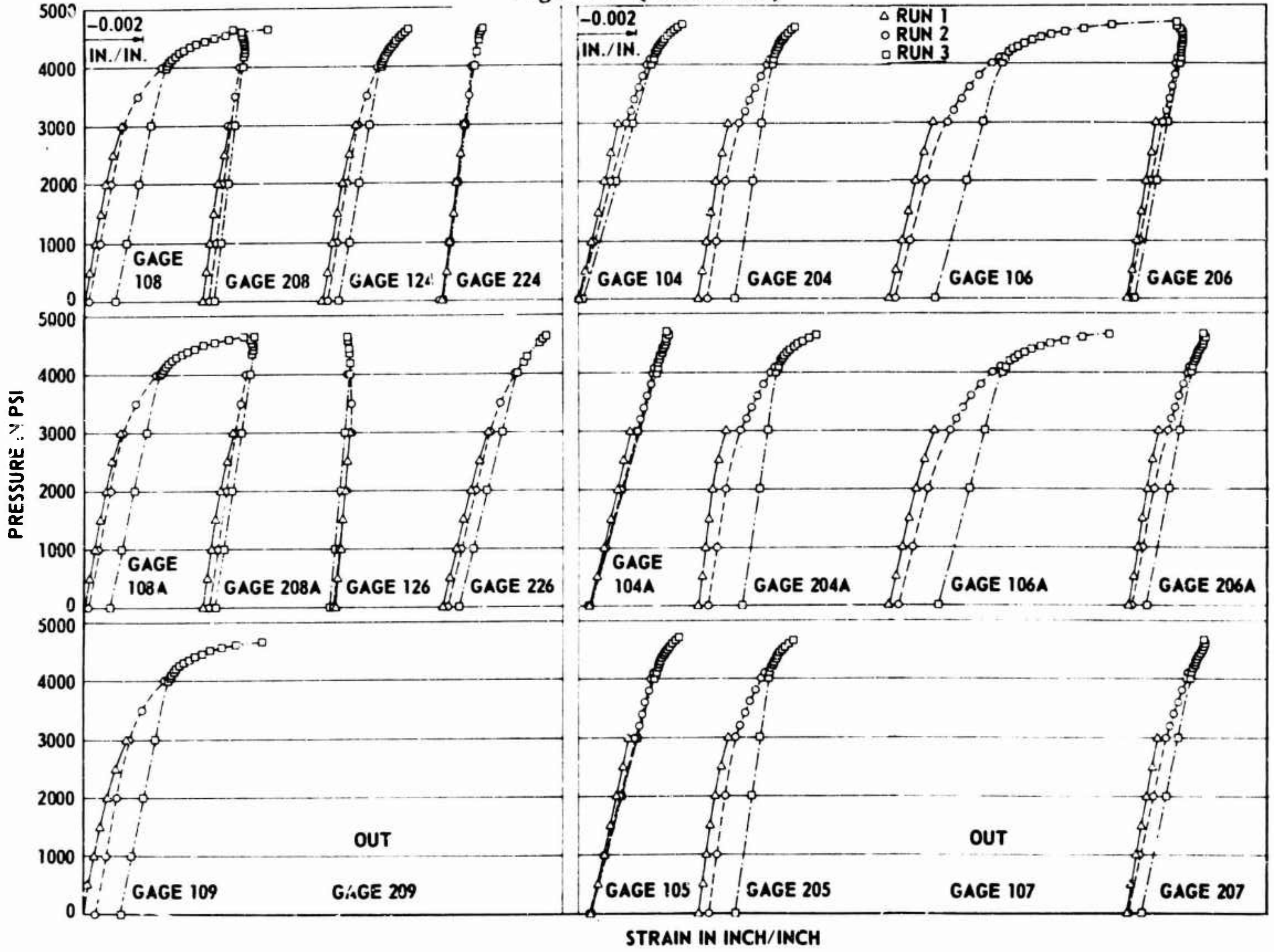

Figure 8 (Continued)

Figure 8g - Model 78

Figure 8h - Model 82

Figure 9 - Models after Collapse

Figure 9a - Model 75

Figure 9b - Model 79

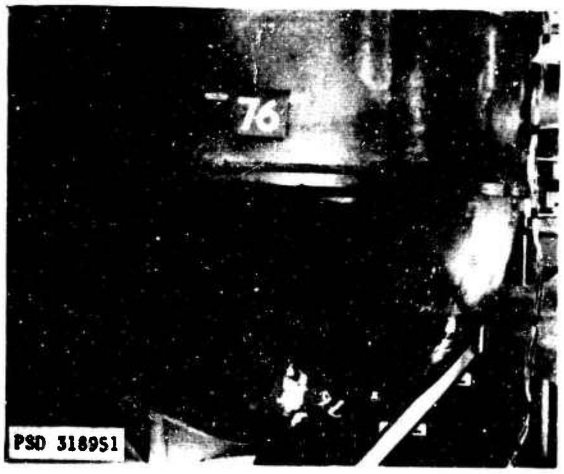

Figure 9c - Model 76

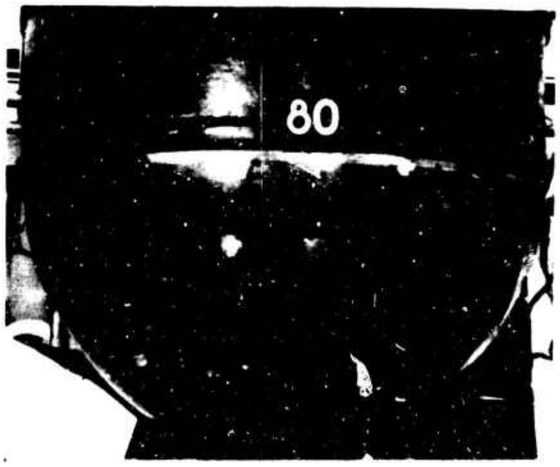

Figure 9d - Model 80

Figure 9e - Model 77

Figure 9f - Model 81

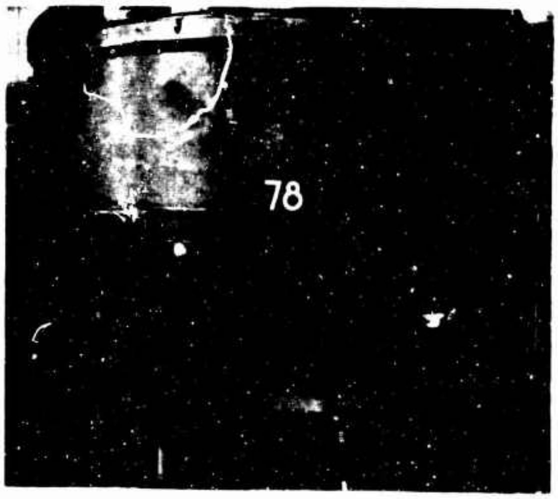

Figure 9g - Model 78

Figure 9h - Model 82

Mismatch on the models could be considered excessive from the viewpoint of possible submarine fabrication tolerances. In most cases, a maximum mismatch of approximately 0.1 in., or roughly 10 percent of the shell thickness, was observed. This caused bending stresses which ranged from 20 to 45 percent of the membrane stress. Unfortunately, the effect of mismatch on collapse strength is somewhat obscured by other variables, and to try to separate its effect is not practical at this time. It should be noted, however, that any effect of mismatch on the strength of the models is reflected in the curves of Figure 10.

On Model 82 (not stress relieved), the question may be raised as to why the result was plotted using the local geometry at IV rather than I (minimum h_a/R_{10}), since both are included in the failure envelope (see Figure 6). Strain measurements taken in these two areas suggest that failure was caused by the flat spot at IV. The higher elastic membrane strains were recorded at IV, and the inelastic strains in this area started to "run" just prior to collapse. Thus, the result for Model 82 was plotted utilizing the local geometry at IV.

The imperfection analysis utilized in evaluating these models admittedly has limitations. For example, failure of some of these models did not occur in the geometrically critical area (minimum h_a/R_{10}). This may be attributed to such factors as varying residual stresses, yield strength, shape of the stress-strain curve, shape of the imperfections, mismatch, and boundary conditions which, at present, are neglected in the analysis. However, the presentation of the data in the form of Figure 10, where each datum point is plotted utilizing the geometry in the area of failure, makes it possible to observe the combined effect of the variables.

In plotting the results of this series of tests for the as-fabricated models, the yield strengths used in conjunction with Equation [2] were determined from material of the original plate.* Discussion in Reference 6 notes that the yield strengths of the original plate material

---

*The data points in Figure 10, which represent the results of the 66-in. diameter models of Reference 6 are based on values of yield strength determined after test, since available yield strength data for the original plating is inadequate.

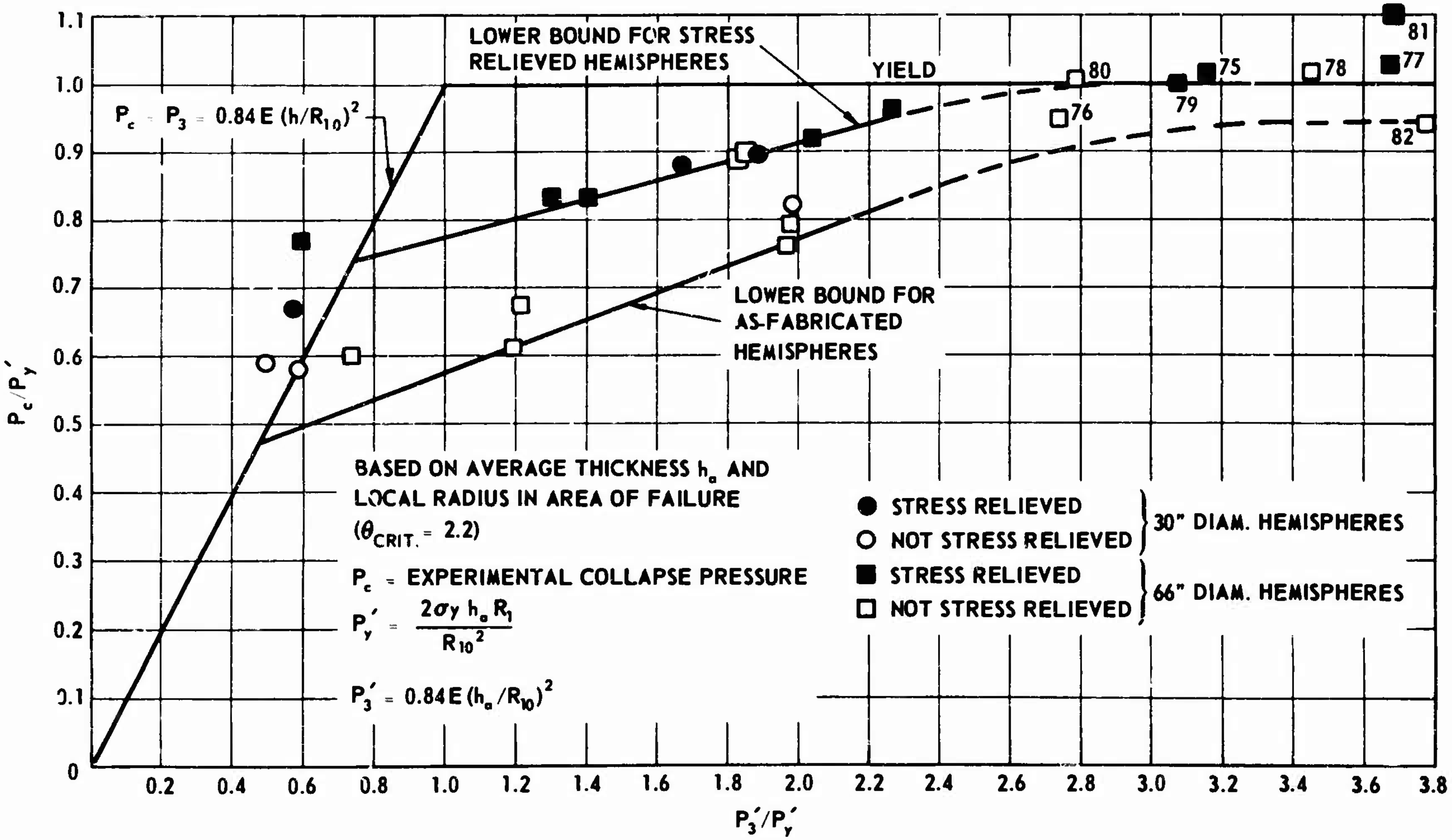

Figure 10 - Nondimensional Plot of Experimental Results for Fabricated HY-80 Steel Spherical Shells

may not be representative of the material in place. The yield strengths of the as-fabricated models were generally 10 percent higher than the stress-relieved models. Since this would affect the position of the data points in Figure 10, it was decided to make a limited investigation of forming on the strength of the material. Specimens were taken from a skirt segment of Model 82 (not stress relieved) between the 0- and 60-deg generators, which appeared to be an area of relatively low stress. The specimen location and test results are presented in Figure 3. Specimens from the model and the original plate were 1/2 in. in diameter by 2 in. in length. For each specimen location, except the center, the yield strength was increased in the direction parallel to the proximate edge and was decreased in the direction normal to it. No significant change in strength was observed at the center of the segment. These results appear to be in contrast with the observations made in Reference 6. Although a maximum increase in strength of 11 percent in the circumferential direction was observed, the strength of the segment in general was not increased by as much as 10 percent. As a matter of fact, if the strength in both directions is averaged for each location as was done in Reference 6, no significant change in strength would be obtained. A closer and more systematic investigation of the effect of forming on the strength of the material is currently in progress. Spherical skirt segments 66 in. in diameter and of varying thicknesses will be fabricated and tested. When these tests are completed, a much clearer understanding of the effect of forming will be obtained.

Typical stress-strain curves of the original plate and from the material in place for Model 82 are presented in Figure 2. Note that in each case cold working of the material altered the shape of the stress-strain curve from one that was essentially elastic and ideally plastic to a curvilinear type. It should be kept in mind that, in machining specimens from the model after testing, stresses are relieved at the free surfaces of the specimens thus making the resulting stress-strain curves only approximate representations of conditions within the model. The effect of residual stress on the elastic behavior of the shell can be observed in the pressure-strain plots presented in Figure 8. The strains in the as-fabricated models become nonlinear at fairly low pressures, whereas the strains in the stress-relieved models remain linear at much higher pressures.

Table 3 compares experimental membrane stress sensitivities at flat spots with values calculated with local imperfection geometry. In most cases the agreement was within 10 percent, with the calculated stresses generally being higher than the measured values. The maximum difference obtained was 14 percent. Considering the relative severity of some of the assumptions made in the analysis (e.g., neglecting nonsymmetric imperfections), the agreement can be considered to be fairly good. At the present time, further study is being conducted on flat spots upon which refinements to the analysis can be based.

Up to the present time, designers of spherical shells have been seriously hampered by the lack of rational design guidance. The preliminary evaluation of the eight model tests, combined with the results of previous tests in the less stable regions, provides the designer with some of these critically needed tools. When the results are presented in the form of Figure 10, the combined effect of the variables--such as residual stress, mismatch, and boundary conditions--can be observed. The curves presented emphasize lower bound strength of test results and are applicable to the realistic design of fabricated spherical shells. At the present time, the effects of flat spots, residual stresses, and mismatch are being investigated both analytically and experimentally. On completion of these investigations, the results of the fabricated HY-80 spherical shells will be reevaluated, and the analysis will be refined. In addition to these studies, the behavior of spherical shells fabricated from materials with strain-hardening characteristics is being investigated.

CONCLUSIONS

1. It was possible to predict within 10 percent the collapse pressures of the eight models tested by utilizing imperfection analysis and extrapolating previous test results of less stable geometries.

2. The test results, when plotted in the form of Figure 10, provide the designer with a reasonable collapse equation for as-fabricated and

TABLE 3

Local Geometry and Comparison of Calculated and Measured Membrane Stresses and Collapse Pressures

Model	Area	h_a inch	$\frac{R_1}{R}$	Calculated Max. Memb. Stress Sens.* psi/psi	Measured Max. Memb. Stress Sens.** psi/psi	Ratio of Calc. to Meas. Stress	Experimental Collapse psi
75***	I	0.810	1.12	23.5	22.2	1.06	
	II	0.807	1.11	23.4	out	--	
	III	0.805	1.10	23.2	21.0	1.05	
	IV†	0.802	1.10	23.3	22.9	1.02	3800
79***	I	0.809	1.19	24.9	out	--	
	II†	0.817	1.15	23.9	23.0	1.04	3650
	III	0.815	1.14	23.7	22.3	1.06	
	IV	0.808	1.12	23.5	out	--	
	V	0.809	1.11	23.3	22.5	1.04	
76	I†	0.789	1.25	26.8	out	--	3150
	II	0.798	1.21	25.7	22.5	1.14	
	III	0.787	1.20	25.8	out	--	
	IV	0.800	1.10	23.4	24.9	0.94	
80	I	0.797	1.27	27.0	24.6	1.10	
	II	0.799	1.26	26.7	24.2	1.10	
	III	0.789	1.23	26.4	23.5	1.12	
	IV	0.797	1.22	26.0	24.8	1.05	
	V†	0.787	1.22	26.3	No Gage	--	3340
77***	I†	1.010	1.19	20.1	20.5	0.98	4490
	II	1.000	1.14	19.5	18.4	1.06	
	III	1.032	1.14	18.9	19.7	0.96	
	IV	1.022	1.14	19.1	19.8	0.96	
	V	1.006	1.13	19.2	18.3	1.05	
81***	I†	1.020	1.20	20.0	18.3	1.09	4800
	II	1.010	1.16	19.6	17.5	1.12	
	III	1.040	1.15	18.9	out	--	
	IV	1.000	1.14	19.5	17.3	1.13	
	V	1.015	1.12	18.9	18.2	1.04	
78	I	0.940	1.18	21.4	out	--	
	II	0.991	1.18	20.3	17.8	1.14	
	III	0.930	1.17	21.4	out	--	
	IV†	0.970	1.15	20.2	out	--	4670
	V	0.983	1.15	20.0	17.7	1.13	
82	I	1.02	1.20	20.2	17.9	1.13	
	II	1.03	1.12	18.7	16.7	1.12	
	III	1.00	1.12	19.2	18.5	1.04	
	IV^{2}	1.03	1.11	18.5	out	--	4750
	V	1.01	1.08	18.4	18.5	0.99	

*The calculated stress sensitivities are determined from the equation

$$\text{Stress sensitivity} = \frac{R_{10}^{\;2}}{2\ h_a\ R_{1m}}$$

**The measured stress sensitivities are based on the average of the strain-sensitivity readings taken on the inside and outside surfaces of the shell. The strain sensitivity is defined as the slope of the portion of the pressure-strain diagram which is linear. Measured stress sensitivities are determined from the expression

$$\text{Stress sensitivity} = \frac{E}{0.2}\left[\frac{\epsilon_1+\epsilon_3}{1-\mu} + \frac{1}{1+\mu}\sqrt{\left(\epsilon_1-\epsilon_3\right)^2 + \left[2\epsilon_2 - \left(\epsilon_1+\epsilon_3\right)^2\right]}\right]$$

where ϵ_1, ϵ_2, and ϵ_3 are the average strain sensitivities at the 0-, 45-, and 90-deg orientation in a three-alament rosatta.

***Stress-relieved model.

†Failure area.

stress-relieved spherical shells with initial imperfections covering the range of geometries of interest to deep submergence.

3. The effects of secondary moments and residual stresses on collapse strength diminish as the ratio of elastic to inelastic buckling pressure of the shell increases.

4. The agreement between calculated and measured membrane stresses at flat spots was fairly good. In most cases the agreement was within 10 percent, while the maximum difference was 14 percent.

ACKNOWLEDGMENTS

The authors wish to express their appreciation to Mr. T.J. Kiernan for his continued interest in the conduct of this project. The assistance of Mr. R.M. Charles in directing the fabrication, instrumentation, and testing of the models is also acknowledged.

REFERENCES

1. Krenzke, M.A., "Tests of Machined Deep Spherical Shells under External Hydrostatic Pressure," David Taylor Model Basin Report 1601 (May 1962).

2. Krenzke, M.A., "The Elastic Buckling Strength of Near-Perfect Deep Spherical Shells with Ideal Boundaries," David Taylor Model Basin Report 1713 (Jul 1963).

3. Krenzke, M.A. and Kiernan, T.J., "Tests of Stiffened and Unstiffened Machined Spherical Shells under External Hydrostatic Pressure," David Taylor Model Basin Report 1741 (Aug 1963).

4. Krenzke, M.A. and Kiernan, T.J., "Elastic Stability of Near-Perfect Shallow Spherical Shells," American Institute of Aeronautics and Astronautics Journal, Vol. 1, No. 12, p. 2857 (Dec 1963).

5. Krenzke, M.A. and Kiernan, T.J., "The Effect of Initial Imperfections on the Collapse Strength of Deep Spherical Shells," David Taylor Model Basin Report 1757 (Feb 1965).

6. Kiernan, T.J. and Nishida, K., "The Buckling Strength of Fabricated HY-80 Steel Spherical Shells," David Taylor Model Basin Report 1721 (Jul 1966).

7. Kiernan, T.J., "Predictions of the Collapse Strength of Three HY-100 Steel Spherical Hulls Fabricated for the Oceanographic Research Vehicle ALVIN," David Taylor Model Basin Report 1792 (Mar 1964).

DOCUMENT CONTROL DATA - R & D

(Security classification of title, body of abstract and indexing annotation must be entered when the overall report is classified)

1. ORIGINATING ACTIVITY *(Corporate author)*
Naval Ship Research and Development Center
Washington, D.C. 20007

2a. REPORT SECURITY CLASSIFICATION
Unclassified

2b. GROUP

3. REPORT TITLE
THE INELASTIC BUCKLING STRENGTH OF FABRICATED HY-80 STEEL HEMISPHERICAL SHELLS

4. DESCRIPTIVE NOTES *(Type of report and inclusive dates)*
Final Report

5. AUTHOR(S) *(First name, middle initial, last name)*
Costello, Malcolm G. and Nishida, Kanehiro

6. REPORT DATE
April 1967

7a. TOTAL NO. OF PAGES
45

7b. NO. OF REFS
7

8a. CONTRACT OR GRANT NO.

b. PROJECT NO. S-F013 01 03, Task 0214
S-F013 03 02, Task 1960

c.

d.

9a. ORIGINATOR'S REPORT NUMBER(S)
2304

9b. OTHER REPORT NO(S) *(Any other numbers that may be assigned this report)*

10. DISTRIBUTION STATEMENT
Distribution of this document is unlimited.

11. SUPPLEMENTARY NOTES

12. SPONSORING MILITARY ACTIVITY
1. Special Projects Office
2. Naval Ship Systems Command

13. ABSTRACT

Eight, 66-in.-diameter, fabricated HY-80 steel hemispherical shells designed to fail by inelastic buckling were tested to observe the effects of initial imperfections and residual stresses on elastic behavior and collapse strength. The results demonstrate that the effect of secondary moments and residual stresses on collapse strength diminish as the ratio of elastic to inelastic buckling pressure increases. It was possible to predict the collapse pressures of these models within ±10 percent by utilizing imperfection analysis and extrapolating previous test results of less stable shells. Fairly good agreement was also obtained by using the same imperfection analysis to predict the membrane stresses in the center of the flat spots. Addition of the results of these tests to those obtained on shells in the less stable regions provides a basis for a reasonable collapse equation for practical spherical shells over the range of shell stability of interest to deep submergence.

DD FORM 1 NOV 65 1473 (PAGE 1)
S/N 0101-807-6801

UNCLASSIFIED
Security Classification

14. KEY WORDS	LINK A		LINK B		LINK C	
	ROLE	WT	ROLE	WT	ROLE	WT
Spherical Shells						
Elastic Buckling						
Inelastic Buckling						
Initial Imperfections						
Residual Stresses						
Critical Local Geometry						

UNCLASSIFIED
Security Classification